J. Membrane Biol. 55, 29–51 (1980)

The Journal of
Membrane Biology

The Malonyl Gramicidin Channel: NMR-Derived Rate Constants and Comparison of Calculated and Experimental Single-Channel Currents

D.W. Urry, C.M. Venkatachalam, A. Spisni, R.J. Bradley, T.L. Trapane, and K.U. Prasad

Laboratory of Molecular Biophysics and Neuroscience Program, University of Alabama Medical Center, Birmingham, Alabama 35294

Summary. Malonyl gramicidin is incorporated into lysolecithin micelles in a manner which satisfies a number of previously demonstrated criteria for the formation of the transmembrane channel structure. By means of sodium-23 nuclear magnetic resonance, two binding sites are observed: a tight site and a weak site with binding constants of approximately $100\,\text{M}^{-1}$ and $1\,\text{M}^{-1}$, respectively. In addition, off-rate constants from the two sites were estimated from NMR analyses to be $k_{\text{off}}^{t} \simeq 3 \times 10^5/\text{sec}$ and $k_{\text{off}}^{w} \simeq 2 \times 10^7/\text{sec}$ giving, with the binding constants, the on-rate constants, $k_{\text{on}}^{t} \simeq 3 \times 10^7/\text{M sec}$ and $k_{\text{on}}^{w} \simeq 2 \times 10^7/\text{M sec}$.

Five different multiple occupancy models with NMR-restricted energy profiles were considered for the purpose of calculating single-channel currents as a function of voltage and concentration utilizing the four NMR-derived rate constants (and an NMR-limit placed on a fifth rate constant for intrachannel ion translocation) in combination with Eyring rate theory for the introduction of voltage dependence.

Using the X-ray diffraction results of Koeppe et al. (1979) for limiting the positions of the tight sites, the two-site model and a three-site model in which the weak sites occur after the tight site is filled were found to satisfactorily calculate the experimental currents (also reported here) and to fit the experimental currents extraordinarily well when the experimentally derived values were allowed to vary to a least squares best fit. Surprisingly the "best fit" values differed by only about a factor of two from the NMR-derived values, a variation that is well within the estimated experimental error of the rate constants.

These results demonstrate the utility of ion nuclear magnetic resonance to determine rate constants relevant to transport through the gramicidin channel and of the Eyring rate theory to introduce voltage dependence.

The primary structure of malonyl gramicidin (malonyl-bis-desformyl gramicidin) is $CH_2(CO\text{-L}\cdot\text{Val}_1\text{-Gly}_2\text{-L}\cdot\text{Ala}_3\text{-D}\cdot\text{Leu}_4\text{-L}\cdot\text{Ala}_5\text{-D}\cdot\text{Val}_6\text{-L}\cdot\text{Val}_7\text{-D}\cdot\text{Val}_8\text{-L}\cdot\text{Trp}_9\text{-D}\cdot\text{Leu}_{10}\text{-L}\cdot\phi_{11}\text{-D}\cdot\text{Leu}_{12}\text{-L}\cdot\text{Trp}_{13}\text{-D}\cdot\text{Leu}_{14}\text{-L}\cdot\text{Trp}_{15}\text{-NHCH}_2\text{-CH}_2\text{OH})_2$ where ϕ_{11} = Trp/Phe/Tyr at the approximate ratios 7:1:2, respectively, and where the L-valyl residue in position one is also replaced to a few percent by an L-isoleucyl residue (Sarges & Witkop, 1964). It is formed by the by the bifunctional malonyl coupling to two desformylated gramicidin molecules (Urry, et al., 1971; Bamberg & Janko, 1977). Malonyl gramicidin was first synthesized in this laboratory for the purpose of testing the proposed head-to-head (amino end to amino end) dimerization for transmembrane channel formation. The synthetic dimer, verified to be pure to within a few percent by proton nuclear magnetic resonance, was utilized in the valuable planar lipid bilayer approach begun by Mueller and Rudin (1967) and was found in terms of concentration to be an exceptionally potent ion transport molecule due to an altered concentration dependence of conductance and conductance development from a second-order to a first-order process (Urry et al., 1971). These results were verified and skillfully extended by Bamberg and Janko (1977) to compare channel mean lifetimes and single-channel conductances resulting from the monomer of gramicidin and the covalent malonyl dimer. The malonyl dimer of gramicidin forms transmembrane channels which can conduct $10^{6.5}$ sodium ions/sec. (reported here) or 10^7 cesium ions/sec (Bamberg & Janko, 1977) at 100 mV, 1 M chloride salt and 25 °C.

The gramicidin channel formation proposed in 1971 (Urry et al., 1971; Urry, 1971) to be the head-to-head hydrogen bonded dimerization of two helical monomers is now well-documented (Urry et al., 1971; Bamberg, Apell & Alpes, 1977; Bamberg & Janko, 1977; Weinstein, et al., 1979). The proposed channel

0022-2631/80/0055-0053 $03.20

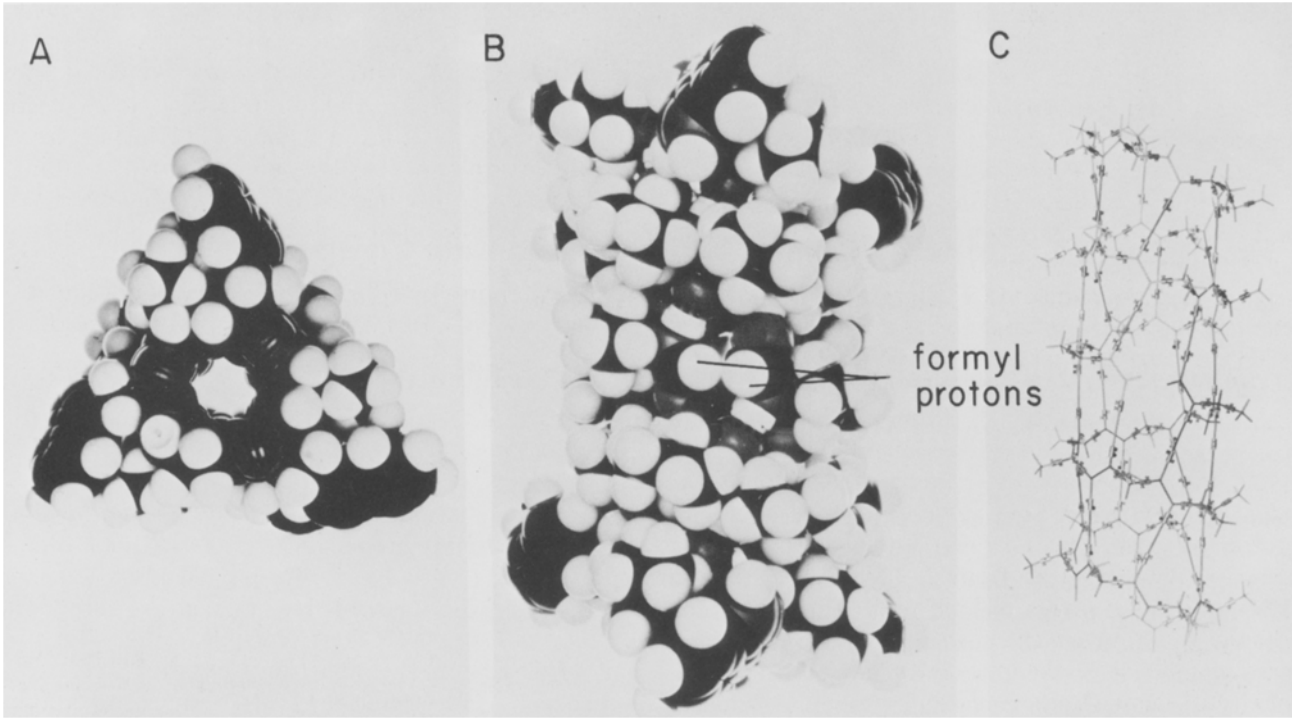

Fig. 1. The gramicidin transmembrane channel structure comprised of two molecules hydrogen bonded head to head (amino end to amino end). (*A*): Channel view showing the 4-Å diameter channel which is continuous for 26 Å. (*B*): Side view showing at center the two formyl protons juxtaposed. In forming the covalent dimer, malonyl gramicidin, the two formyl protons are replaced by a methylene moiety, CH_2. (*C*): Wire model of channel in side view. (From Urry et al., 1975)

structure (Urry et al., 1971; Urry, 1973) has a 4-Å diameter channel which is coincident with the helix axis. Utilizing our previously published approximate coordinates (Urry, 1973), the density weighted mean diameter of the backbone atoms of the helix would be 6.9 Å and the length would be about 26 Å. The latter value derives from the dipeptide translation length of 1.6 Å (*see* Table of $\beta^6_{3,3}$-helix parameters in Urry, 1973) because there are 16 peptide moiety pairs per channel giving $(1.6 \times 16 =) 25.6$ Å. Accordingly, when treating the issue of an optimal lipid layer thickness, a value of 26 Å has been considered (*see* Fig. 6 of Urry et al., 1975). Perspectives of the gramicidin channel are given in Fig. 1.

Although the published crystal structure studies from the Stryer group are as yet at limited resolution, they have demonstrated a conformational change on K^+ and Cs^+ complexation with the two complexes being isomorphous (Koeppe et al., 1979). The ions are observed within the channel of a helix with a 6.8 Å diameter and a 26 Å length, within tenths of an Angstrom of the previously defined $\beta^6_{3,3}$-helical parameters (Urry, 1973; Urry et al., 1975). An important aspect of the crystal structure studies for the present effort are the ion locations, or binding sites, within the channel. The X-ray studies indicate two ion binding sites per channel length of 26 Å which are separated by 21 and 5 Å along the end-to-end aligned channels. This places ion binding sites 2.5 Å from an end of a component monomer but from which end, the amino or carboxyl, is not resolved (Koeppe et al., 1979). As crystallization was carried out with approximately equimolar gramicidin and cation concentrations, this defines what are referred to in the present study as the tight binding sites. The two options are for the tight binding sites to occur 2.5 Å from each carboxyl terminus of the amino end-to-amino end dimer and therefore separated by $(26 - 2 \times 2.5 =)$ 21 Å, or 2.5 Å from each amino end and therefore, in the amino end-to-amino end dimer, separated by 5 Å. Since the sites are the same for Cs^+ and K^+ and since the crystal radius of Cs^+ is 1.69 Å, this would place two ions with their close contact surfaces separated by only 1.62 Å which is not enough room for a single water molecule. Such a situation could be expected to result in a large repulsion energy. For this reason the situation of sites separated by 5 Å is taken to be the definition of degenerate sites which cannot be simultaneously occupied. These considerations are basic to the discussions below and in Appendix A on the various multiple occupancy models and on the correct in-

troduction of voltage dependence to the nuclear magnetic resonance-derived rate constants.

Early approaches for characterizing the conformation of the gramicidin channel and its cation interactions in organic solvents have been limited due to the presence of multiple conformations (Urry et al., 1975) and because the ion binding properties did not correlate well with ion transport properties (Urry, 1978). In trifluoroethanol, for example, where the conformation is thought to be more nearly that of the channel state, there is observed almost no interaction with Na^+ or K^+ while a strong complexation is observed with Ca^{2+} (Urry, 1978), whereas the channel interactions relevant to transport in planar bilayers indicate just the reverse (Bamberg & Läuger, 1977). As a means of overcoming these limitations, recent efforts have been directed toward incorporation of gramicidin channels into lysolecithin micelles (Urry, Spisni & Khaled, 1979*a*; Urry et al., 1979*b*). The advantage of lipid micelle packaging of channels is that the characterization of ion binding sites would not be complicated by the development of electrochemical potentials which would occur during ion titrations of channels in vesicles. The arguments for the channel state in phospholipid micelles (Urry et al., 1979*a*, *b*) are (i) that there is a correlation of the onset of Na^+ interaction with perturbation of the lipid core, (ii) that there is competitive binding of Ag^+ and Tl^+ which displaces the Na^+ interaction in the micellar packaged gramicidin and Ag^+ and Tl^+ exhibit competitive block of Na^+ transport in planar lipid bilayer studies (McBride & Szabo, 1978; Neher, 1975; Sandblom, Eisenman & Neher, 1977), and (iii) that the activation energy for Na^+ exchange with the micellar packaged gramicidin at equimolar Na^+ and channel concentrations (as measured by temperature dependence of sodium-23 line width and longitudinal relaxation time) is the same as the activation energy for transport through the channel (Bamberg & Läuger, 1974). The latter point provides the useful argument that the energy barriers for intrachannel ion translocations can be no greater than the barrier for the ion leaving the channel from the tight site.

Previous sodium-23 nuclear magnetic resonance studies on micellar packaged gramicidin have identified two sodium binding sites (a tight site, $K_b^t \simeq 100\,\text{M}^{-1}$ and a weak site $K_b^w \simeq 3\,\text{M}^{-1}$) as well as the approximate off rate constants from these binding sites, $k_{\text{off}}^t \simeq 3 \times 10^5$/sec and $k_{\text{off}}^w \simeq 4 \times 10^7$/sec (Urry et al., 1980). The resulting four rate constants ($K_b = k_{\text{on}}/k_{\text{off}}$) along with a fifth rate constant, that, by the above argument of activation energy, must be greater than k_{off}^t, have been utilized in combination with Eyring rate theory and steady-state equations for two and three site occupancy models to calculate the gramicidin single-channel currents with satisfying correspondence between the electrical measurements on planar bilayers and the calculated currents. Because the gramicidin study is complicated by the degree of gramicidin incorporation into lysolecithin micelles and by the possible presence of ion binding monomers, the malonyl gramicidin dimer has been used in the present study and calculational and analytical details not possible in the shorter report on gramicidin are included in this report. Additionally, as the malonyl gramicidin ion currents are significantly less than those of gramicidin (Bamberg & Janko, 1977), it is of interest to determine if this difference is assessable in differences in the NMR-derived constants.

Materials and Methods

A. Synthesis of Malonyl Gramicidin

Commercially available gramicidin was purchased from Nutritional Biochemicals Corporation, Cleveland, Ohio. This product contains approximately 72% gramicidin A (Trp_{11}), 9% gramicidin B (Phe_{11}) and 19% gramicidin C (Tyr_{11}). Ion exchange resins were obtained from Bio-Rad Laboratories, Richmond, Calif.

Malonyl-bis-desformyl gramicidin: The preparation of the gramicidin derivative (Urry et al., 1971; Bamberg & Janko, 1977) was carried out by the following procedure. Desformylgramicidin was obtained from gramicidin by following essentially the procedure of Ishii and Witkop (1964) except that the acidolysis step was carried out in the presence of a nitrogen atmosphere for 2 hr. The product was purified by ion-exchange chromatography on a column of AG 50W-X2 (H+ form) resin. Desformylgramicidin (10% excess) dissolved in DMF was reacted with di-*p*-nitrophenylmalonate (Backer & Lolkema, 1938), prepared by refluxing malonic acid, *p*-nitrophenol and phosphorus oxychloride (Parihar, Sharma & Verma, 1967) over a period of 48 hr. The pH of the reaction mixture was maintained slightly above 7 by adding N-methyl morpholine. DMF was removed under reduced pressure; the residue was taken in methanol and passed through a column of AG 501-X8(D) mixed bed resin and then through a column of AG 50W-X2 (H+ form) resin. The malonyl-bis-desformyl gramicidin thus obtained was further purified by gel filtration over a Sephadex LH-20 column using methanol for elution. Purity of the product was checked by thin layer chromatography (solvent system, $CHCl_3/CH_3OH/H_2O$, 65:25:4) and proton magnetic resonance (Urry et al., 1971) and carbon-13 magnetic resonance (CMR) spectra. The absence of the formyl group carbonyl carbon frequency and the presence of the $\underline{C}=O$ frequency of the malonyl group could be verified in the CMR spectra. The presence of the malonyl group was also confirmed by synthesizing ^{13}C enriched ($CH_2-(\underline{C}O)_2$) malonyl-bis-desformyl gramicidin where malonyl by-products could also be identified with high sensitivity.

B. Incorporation of Malonyl Gramicidin into Lysolecithin Micelles

The source of egg yolk lysolecithin, containing primarily palmitic and stearic acid in position 1, was Sigma Chemical Company, St. Louis, Mo.; it was used without further purification. The studies were carried out in 99.7% D_2O (Merck & Co., St. Louis, Mo.) in order

that the deuterium could be used as a lock signal for the nuclear magnetic resonance studies. Sonication, by means of a Branson cell disruptor model W-225R for 3 min at power 3 employing a cup horn accessory, was used to disperse the lysolecithin micelles in D_2O. A measured quantity of malonyl gramicidin was then added to result in a concentration of approximately 3 mM. After shaking the suspension with a Vortex mixer for several minutes, it was sonicated for 6 min at power 4. Following the procedure previously used to achieve a stable channel-like state for gramicidin (Urry et al., 1979*b*), the sample was heated for more than 12 hr at 60–70 °C. The sample used in the T_1, chemical shift, and line width experiments was incorporated after addition of 0.5 mM NaCl, while the sample used in the T_2 and line shape analyses was incorporated after addition of 5.76 mM NaCl. Malonyl gramicidin appeared to incorporate more readily than gramicidin as judged by a shorter time required to achieve a clearing of the suspension.

C. *Sodium-23 Nuclear Magnetic Resonance Methods*

1. Instrumentation

^{23}Na NMR data were measured at 26.3 MHz on a JEOL FX-100 spectrometer equipped with a 10-mm multinuclear probe and operating with a deuterium lock. The probe temperature was maintained at 30.5 ± 2 °C by a JEOL VT-3B temperature controller and was measured directly in the sampling area by a Fluke temperature probe. The spectrometer was operated in the pulse-Fourier transform mode by a Texas Instruments 980B computer (48 K memory) with foreground-background data acquisition and analysis capability, utilizing a Diablo 31, 1.14 megaword capacity, disk system for data and program storage. The ^{23}Na signal was collected as a free induction decay from the probe via a direct memory access channel (background) to the CPU. All data analysis and relaxation time calculations were carried out in the foreground of the computer.

2. Longitudinal Relaxation Studies

Experimental. ^{23}Na longitudinal relaxation times (T_1) were obtained using the inversion recovery method ($180° - \tau - 90°$ pulse sequence). The 180° pulse width for the micellar-malonyl gramicidin-NaCl system was determined as the pulse that gave no detectable ^{23}Na signal. A delay time of 400 msec ($> 5 \times T_1$) was allowed after each pulse sequence for complete return to thermal equilibrium. The T_1's at each NaCl concentration were calculated using from seven to nine partially relaxed spectra collected at various pulse intervals (τ). The pulse interval for complete relaxation was also taken as greater than $5 \times T_1$. The relaxation time for free ^{23}Na was measured for 10 mM NaCl in D_2O at 30.5 ± 2 °C to be 57 msec and for 10 mM NaCl plus lysolecithin micelles at the same temperature to be 49 msec.

Data Analysis. For ^{23}Na exchanging between a free state f in solution and a bound state b, the longitudinal relaxation rate R_1 is given by

$$R_1 = 1/T_1 = P_f R_{1f} + P_b R_{1b} \tag{1}$$

where R_{1f} and R_{1b} are the ^{23}Na longitudinal relaxation rates at the states f and b. The excess relaxation rate is then

$$R_1 - R_{1f} = P_b(R_{1b} - R_{1f}). \tag{2}$$

Following James and Noggle (1969), when the total site concentration, C_T, is much less than the total sodium concentration, Na_T,

$$(R_1 - R_{1f})^{-1} = \frac{1}{C_T(R_{1b} - R_{1f})}[Na_T + K_b^{-1}] \tag{3}$$

such that a plot of the reciprocal of the differential rate, $(R_1 - R_{1f})^{-1}$, against the total ion concentration will be a straight line for a simple binding process and the extrapolated negative x-axis intercept will provide the reciprocal of the binding constant, $(K_b)^{-1}$. The value of R_{1f} of 20.4 sec^{-1} was determined for the same lysolecithin micelle concentration in the absence of malonyl gramicidin.

3. Transverse Relaxation Studies

Experimental. ^{23}Na transverse relaxation times (T_2) were obtained using the Carr-Purcell-Meiboom-Gill pulse sequence $(90° - (\tau - 180° - \tau)_n)$. The 180° pulse width was determined as for T_1 measurements. The maximum ^{23}Na signal was detected following the shortest delay after the 90° pulse allowing for instrument recovery time, and then successive spectra were collected at longer pulse intervals (τ) to observe the relaxation in the transverse plane. A 300-msec delay time was allowed for equilibration after each pulse sequence. Spectra were collected over four overlapping regions of varying τ in order to completely describe the decay of the signal. The transverse relaxation time for free ^{23}Na (T_{2f}) was measured for 10 mM NaCl in D_2O at 30.5 ± 2 °C in the presence of lysolecithin micelles and was found to be 50 msec.

Data Analysis. Under certain conditions the decay of the transverse magnetization is experimentally found to be nonexponential. This observation is explicable by the theoretical analyses of Hubbard (1970), Bull (1972), and Bull et al. (1973) who have shown that for a quadrupole-relaxed spin-3/2 nucleus, such as ^{23}Na, the decay of the transverse magnetization is given by

$$M_t = M_o[0.6\exp(-t/T_2') + 0.4\exp(-t/T_2'')] \tag{4}$$

where T_2' and T_2'' are the fast and slow components of the transverse relaxation times, when the extreme narrowing condition is not satisfied at the binding site. Our interest in these two components is that they are related to the correlation time, τ_c, at the binding site as follows (Bull, 1972; Bull et al., 1973; Norne et al., 1979):

$$1/T_2' = 1/T_{2f} + P_w\frac{\chi^2}{20}\left[\tau_c + \frac{\tau_c}{1+\omega^2\tau_c^2}\right] \tag{5a}$$

and

$$1/T_2'' = 1/T_{2f} + P_w\frac{\chi^2}{20}\left[\frac{\tau_c}{1+4\omega^2\tau_c^2} + \frac{\tau_c}{1+\omega^2\tau_c^2}\right] \tag{5b}$$

where χ is the quadrupole coupling constant at the weak site and $\omega = 16.5 \times 10^7$ rad/sec. A T_{2f} of 50 msec was obtained on a suspension of lysolecithin micelles in the absence of malonyl gramicidin. From Equations (5*a*) and (5*b*) one obtains the following relationship between relaxation times and the correlation time:

$$\frac{1/T_2' - 1/T_{2f}}{1/T_2'' - 1/T_{2f}} = \frac{1 + 1/(1+\omega^2\tau_c^2)}{1/(1+4\omega^2\tau_c^2) + 1/(1+\omega^2\tau_c^2)}. \tag{6}$$

Using this equation, τ_c may be computed if T_2' and T_2'' are known. Once τ_c is known, the off-rate is readily computed, since $k_{off}^w \simeq 1/\tau_c$ (Cornélis & Laszlo, 1979). Thus, with determination of the two relaxation time components, it becomes possible to evaluate an off-rate constant under conditions where Eqs. (5) and (6) apply.

Determination of T_2' and T_2'' for the Nonexponential Relaxation. The fast and the slow components of the transverse (nonexponential) relaxation may be achieved by two alternative methods. One method makes use of the direct determination of the decay of the transverse magnetization with time while the other consists of analyzing the non-Lorentzian line shape that results from such nonexponential relaxation.

Curve-Stripping. Experimentally one may directly observe the variation of the transverse magnetization, M_t, with time t, then fit the resulting plot of M_t *vs.* t to Eq. 4 by least-square analysis, and obtain T_2' and T_2'' (Chang & Woessner, 1978).

Deconvolution of the NMR Line-shape. Owing to the presence of two components for the transverse relaxation, the ^{23}Na NMR line signal is found to be distinctly non-Lorentzian. In fact, the line signal is simply a sum of two different Lorentzians, one due to the fast component with line-width of $1/\pi T_2'$ and the other narrow Lorentzian due to the slow component with a line width of $1/\pi T_2''$. The line-widths of the broad and narrow components can be obtained from $\nu_{1/2}$, the width at half height, and $\nu_{1/8}$, the width at (1/8)th of the actual line signal, by following an interesting method described by Delville, Dettellier and Laszlo (1979). Alternatively, one may perform a full deconvolution of the non-Lorentzian line signal into its broad and narrow components. The results of the Lazlo method (Delville et al., 1979) and the full deconvolution will be compared.

4. Concentration Dependence of Chemical Shift and Line Width

Experimental. The ^{23}Na chemical shift at varying NaCl concentrations in the micellar malonyl gramicidin system was calculated using, as the reference at 0 ppm, the signal from 10 mM NaCl in D_2O (free sodium), under equivalent experimental and instrumental conditions. In all cases the chemical shift for ^{23}Na in the presence of micellar-malonyl gramicidin is negative, as the free sodium signal occurs at lower field than the bound sodium. Since the T_{2f} (50 msec) for free ^{23}Na in the presence of micelles corresponds to a line width at half signal height of 6 Hz and the experimentally observed line width was found to be approximately 10 Hz, the difference of 4 Hz instrumental line broadening is taken as due to magnetic field inhomogeneity. These corrections will be taken into considerations in the Laszlo line shape and signal deconvolution calculations

Data Anqlysis. The variation of chemical shift and line width with total sodium concentration can also be used to characterize a binding process and can be particularly useful in separating out a tight binding process which may dominate at low ion concentrations. The expressions for the chemical shift, ν (in Hz), and line width, $\nu_{1/2}$ (in Hz), are quite simple if the exchange at a tight site is sufficiently rapid. Assuming the fast exchange condition (Pople, Schneider & Bernstein, 1959; Binsch, 1968; Feeney et al., 1979), we may write

$$\nu = P_f \nu_f + P_t \nu_t; \quad K_b^t = \text{function } (P_f, P_t) \tag{7}$$

and

$$\nu_{1/2} = \nu_{1/2}^f + P_t(\nu_{1/2}^t - \nu_{1/2}^f) + 4\pi P_t(1-P_t)^2 \frac{\nu_t^2}{k_{\text{off}}^t}. \tag{8}$$

Both the line width and chemical shift data may be least-squares fitted to Eqs. (7) and (8) in order to obtain values for K_b^t, ν^t, $\nu_{1/2}^t$ and k_{off}^t.

Line Width vs. Chemical Shift Plot. The role played by the off-rate, k_{off}^t, is demonstrable by considering a line-width *vs.* chemical shift plot (*see* Results). By combining Eqs (7) and (8) one may eliminate P_t to obtain the relation, with $\nu_f = 0$, of

$$\nu_{1/2} = \nu_{1/2}^f + \frac{\nu}{\nu_t}(\nu_{1/2}^t - \nu_{1/2}^f) + \frac{4\pi\nu(\nu_t - \nu)^2}{\nu_t k_{\text{off}}^t}. \tag{9}$$

For a given ν^t and $\nu_{1/2}^t$, the shape of this plot depends on the off-rate, k_{off}^t. Additionally, the fast exchange assumption can be checked or corrected with use of the more general expressions of Feeney et al. (1979) – *see* Eqs. (9)–(11) of that paper.

D. Measurement of Single-Channel Currents

Optically black lipid membranes were formed in a Teflon chamber as previously described (Bradley et al., 1977; Bradley et al., 1978). The lipid used was 1% (wt/vol) diphytanoyl phosphatidyl choline in *n*-decane. The lipid bilayer membrane area was about 2×10^{-3} cm^2 for the single-channel measurements. A Tektronix storage oscilloscope was used to store the single channel events and 10 or more events were averaged for a given membrane. The sodium chloride concentrations used were 0.1, 1, 3, and 5.5 M. The activity coefficients for conversion to molal activities were obtained from Harned and Owen (1958), and the studies were carried out at 25 °C for 50, 100, 150, and 200 mV.

E. Calculation of Single-Channel Currents using NMR-Derived Rate Constants

In an approach similar to that employed by Sandblom et al. (1977) the channel is considered as occurring in a number of different states, depending on the number and location of ions in the channel. Taking the probability of a given channel state, or equivalently the fraction of time that a channel is in a particular state, as χ_i for $i = 0, 1 \ldots n$ states where χ_o, for example, represents the probability of the unoccupied channel, the single-channel current, I_x, due to the x ion may be written

$$I_x = z e \sum_i \sum_j \underline{\lambda}_{ij} q_{ij} \chi_i \tag{10}$$

where z is the valency or unit charge on ion x and e is the number of coulombs per unit charge, i.e., 1.6×10^{-19} C. The quantity $\underline{\lambda}_{ij}$ is the fraction of total channel length which changes with the rate q_{ij} χ_i where the summation over j involves all those rate processes beginning with state i. The fraction of length $\underline{\lambda}_{ij}$ may be viewed as a one dimensional vector quantity which is positive for movement down the potential gradient and negative for movements against the potential gradient. The units of q_{ij} are sec^{-1}; for first-order processes q_{ij} is the rate constant, and for second-order processes it is the product of the ion molar activity times the second-order rate constant with units (Msec)$^{-1}$.

By way of example, consider the two-site model of the channel with the four states oo, xo, ox and xx and the single channel current Eq. (A2) of Appendix A. The unoccupied channel state, oo, has the probability, $\chi(oo)$, equivalent to χ_o of Eq. (10); state χ_1 would be the singly occupied state, $\chi(xo)$, etc. The q_{ij} for the oo state in Eq. (A2) are $C_x' k^1$ for the entry of the ion from the positive side of the membrane and $C_x'' k^{-2}$ for entry from the negative side and the associated $\underline{\lambda}_{ij}$ are the signed length ratios $(d - a_1)/2d$ and $-(d - a_1)/2d$, respectively, where the lengths are defined in Fig. A-1*b*. As a sample calculation, consider the contribution to the current of the term $z e(2a_1/2d) k^5 \chi(xo)$ of Eq. (A2) which would be the term $z e \underline{\lambda}_{11} q_{11} \chi_1$ of Eq. (10). For a sodium ion $z = 1$; for the

two-site model (*see* Figure A-2*b*) $(2a_1/2d)=21/26$; and somewhat arbitrarily choosing the situation where $\chi(xo)=0.3$ and $k^5=10^7\,\text{sec}^{-1}$ gives

$$(I_x)_{11}=(1.6\times10^{-19}\,\text{C})(0.81)(10^7/\text{sec})(0.3)$$
$$=3.9\times10^{-13}\,\text{C/sec}.$$

At a transmembrane potential, E, of 100 mV and with the relation, $I=E/R=EG$ where R is the resistance and G is the conductance, this gives a contribution to the conductance of 3.9×10^{-12} C/V sec or 3.9 pS.

For a given occupancy model, the set of χ_i of the steady-state equations, i.e., of Eqs (A1), (A5), (A7), (A10) and (A12) for the five models considered here, can be solved in terms of voltage-dependent rate constants and concentrations with the addition of the conservation Eq. (B2), as outlined in Appendix B. Accordingly, our next concern is to outline the means of introducing voltage dependence into the NMR-derived rate constants.

Rate Theory Conversion of NMR-derived Rate Constants to Voltage Dependent Rate Constants. Following Eyring rate theory (Zwolinski, Eyring & Reese, 1949; Johnson, Eyring & Polissar, 1954; Parlin & Eyring, 1954; Eyring & Urry, 1963; 1965), the free energy change for moving an ion from one side to the other of a membrane, across which is applied a voltage, is zFE where z again is the charge on the ion, F is the Faraday and E is the potential or electromotive force. On applying a voltage across a membrane the cations on the positive side are raised by $zFE/2$ and lowered by an equivalent amount on the negative side. Our present concern is the change in free energy profile for crossing the membrane which is brought about by the applied potential. For simplicity it is assumed that the potential gradient is linear. This means, of course, that the free energy change due to the applied potential would be zero at the center of the membrane. This is strictly correct for the ion transport of interest here because the membrane is a symmetrical lipid bilayer and because the ion channel has two-fold symmetry perpendicular to its channel axis. Also considering the most immediately involved backbone atoms of the helical channel, linearity remains a good approximation since in each monomer there are 16 peptide moieties which alternately point parallel and antiparallel to the helix axis. It is necessary to go to the side chains of the helix before a significant perturbation of linearity could be anticipated because of the tryptophan residues being clustered near the carboxyl end of the channel. Because of the particular structure of the gramicidin channel, an assumed linearity of the potential gradient is not an unreasonable first-order approximation. Accordingly, the factor by which the NMR-derived rate constants should be multiplied is $\exp(\ell zFE/2dRT)$ where $2d$ is the length over which the potential is applied and ℓ is a length along the channel from a minimum in the free energy, i.e., a binding site, to the rate limiting barrier for the jump being considered. For convenience, a quantity X is defined as $X\equiv\exp(zFE/2dRT)$ such that the rate constants are multiplied by the quantity X^ℓ where the length is defined by the energy profile for the particular multiple occupancy model being considered (*see* Appendix A). The correct introduction of voltage dependence in the single-channel current equation is checked by verifying that the current is zero when E is zero and that the current exactly reverses when the sign of E is reversed.

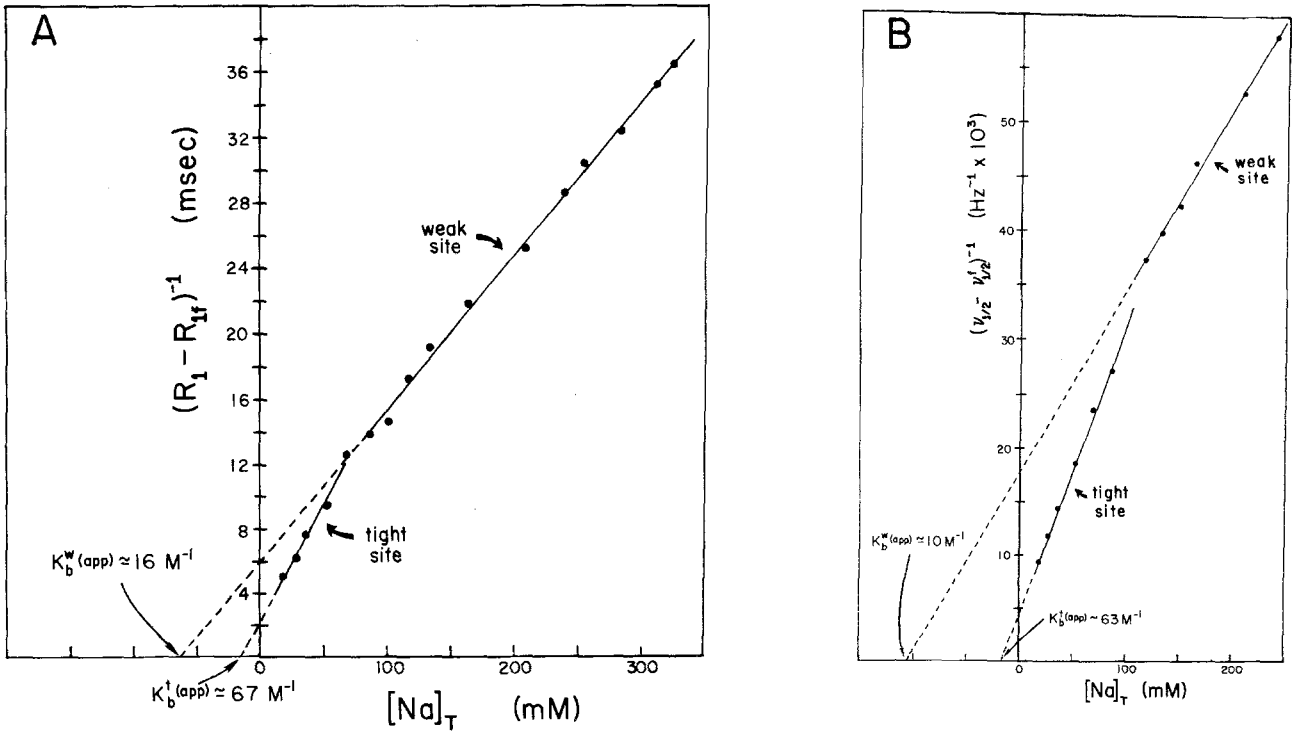

Fig. 2. (*A*): Reciprocal of the excess longitudinal relaxation (ELR) rate plotted against $[Na]_T$, for $C_T\sim2.8$ mM, and $T_{1f}=47$ msec. The nonlinear plot suggests that there are two types of binding sites. Two different straight lines fitted to low and high sodium concentration data are shown. The x-axis intercepts marked yield only "apparent" binding constants. Calculations show that the actual binding constant of the weak site is lower than seen here (*see* text). (*B*): Reciprocal of the excess line width plotted against $[Na_T]$ also showing a "break" around 100 mM, suggesting that there are two types of sites. The resulting "apparent" binding constants closely agree with those obtained from the ELR plot. The line width $\nu_{1/2}^f$ in the channel-free micellar system is 10 Hz. Since $\nu_{1/2}=1/(\pi T_2)$, this plot may be considered to be an excess transverse relaxation (ETR) rate plot

Results

A. Characterization of the Sodium Binding Sites

1. Analysis of the Excess Longitudinal Relaxation Rate (ELR) and Excess Line Width (ELW) Plots

The ELR and ELW plots shown in Fig. 2 provide convincing evidence for the existence of two types of sites. The T_1 data plotted in Fig. 2*a* show the striking feature that the data points, instead of falling on a straight line as is expected when a single binding process is present, are described by a nonlinear curve with the slope decreasing with increasing Na_T. The data points can be fitted to two different straight lines, the one at low concentration range, 15–75 mM, giving an axis intercept of -15 mM, while for the high concentration range, 100–450 mM, a larger intercept of -63 mM is seen. The plot therefore indicates the presence of two types of binding sites, a tight site with an apparent binding constant of $67\,M^{-1}$ and a weak site with apparent binding constant of $16\,M^{-1}$. Owing to the presence of two overlapping binding processes, the actual binding constants may differ. To take into account the presence of the two binding sites, the tight site t and the weak site w, Eq. (2) for the excess rate may be modified as follows:

$$R_1 - R_{1f} = P_t(R_{1t} - R_{1f}) + P_w(R_{1w} - R_{1f}) \qquad (11)$$

where P_t and P_w are fractions of the ions bound to the tight and weak sites, respectively. The exact details of the multiple occupancy model determines the relationship between the fractions bound P_t and P_w and the binding constants K_b^t and K_b^w. Actual binding constants and the relaxation rates R_{1t} and R_{1w} at the binding sites are deduced by least-squares fitting of experimental data in Fig. 2 using Eq. (11). Using the two-site model, the ELR data is best described by Eq. (11) with a $K_b^t = 63\,M^{-1}$, $K_b^w = 1.4\,M^{-1}$, $T_{1t} = 0.5$ msec and $T_{1w} = 0.19$ msec. For a three-site model, the least-square analysis yields the values $K_b^t = 63\,M^{-1}$, $K_b^w = 0.5\,M^{-1}$, $T_{1t} = 0.45$ msec, $T_{1w} = 0.20$ msec. The finding that $T_{1w} < T_{1t}$, i.e., $R_{1w} > R_{1t}$, is consistent with the presence of an ion at the tight site causing a larger fluctuating electric field gradient for the second ion, which results in a faster relaxation rate for the second binding process. The ELW plot in Fig. 2*b* also exhibits similar features, i.e., two sites where apparent binding constants of 63 and $10\,M^{-1}$ are evident.

2. The Off-Rate at the Weak Site

Curve Stripping. The relaxation of the transverse magnetization at $[Na]_T \sim 350$ mM was found to be nonexponential: A plot of $\ln M_t$ *vs.* t turned out to be nonlinear with two different asymptotic slopes at small t and large t, as expected from Eq. (4). The curve was successfully "stripped" to obtain its exponential components, resulting in the values of $T_2' = 0.4 \pm 0.15$ msec and $T_2'' = 8.0 \pm 1.0$ msec. These yielded a value of $(3.0 \pm 1.0) \times 10^7$/sec for the weak off-rate, k_{off}^w.

Line-Shape Analysis. At this high sodium concentration, the shape of the line signal was found to be non-Lorentzian. With $\nu_{1/2} \simeq 38$ Hz and $\nu_{1/8} \simeq 120$ Hz. Correcting for field inhomogeneity and using Laszlo's method (*see* Eqs. (8) and (9) of Norne et al., 1979) gives $T_2' = 0.25 \pm 0.05$ msec and $T_2'' = 8.6 \pm 0.2$ msec giving, $k_{off}^w = (2.1 \pm 0.3) \times 10^7$/sec. When corrected for inhomogeneity the full deconvolution of the line signal yielded the following values: $T_2' = 0.27 \pm 0.05$ msec, $T_2'' = 8.7 \pm 0.2$ msec, $k_{off}^w = (2.3 \pm 0.3) \times 10^7$/sec. Thus, Laszlo's simple method is found to agree very well with the full deconvolution. It may also be noted that the relaxation times obtained from the direct analysis of the decay of the transverse magnetization, M_t, agree reasonably well with those derived from the line shape analysis.

3. Concentration Dependence of Chemical Shift and Line Width

The tight binding site may be further characterized by the variation of chemical shift and line width with $[Na]_T$ at low sodium concentrations (*see* Fig. 3). The tight binding process results in a rather large chemical shift of 22 ppm for $[Na]_T \sim 0.5$ mM with a corresponding line width of ~ 275 Hz. Assuming one tight site per channel molecule (for the two- and three-site models), the best fit to the chemical shift data is obtained for the values $K_b^t = 146 \pm 20$ mM, $\nu_t = 1850 \pm 100$ Hz. The agreement between the calculated curve and the experimental data is quite good for this case. On the other hand, consideration of two tight sites per channel (four-site model) results in the values of $K_b^t = 290 \pm 50$ mM and $\nu_t = 825 \pm 100$ Hz. However, as shown in Fig. 3, the fitting in this case is not as good as the previous models with one tight site per channel. Thus, the chemical shift data analyzed by Eq. (7) seems to support two- and three-site models and, as will be seen later, the four-site model does not give rise to the experimental currents.

Similarly, the line width data also characterizes the tight binding site. An approximate value of the line width at the binding site is obtained by fitting the line width data to Eq. (8), neglecting the third term (exchange term) of that equation. This analysis yields $K_b^t \simeq 125\,M^{-1}$ and $\nu_{1/2}^t \simeq 995$ Hz. The actual line width

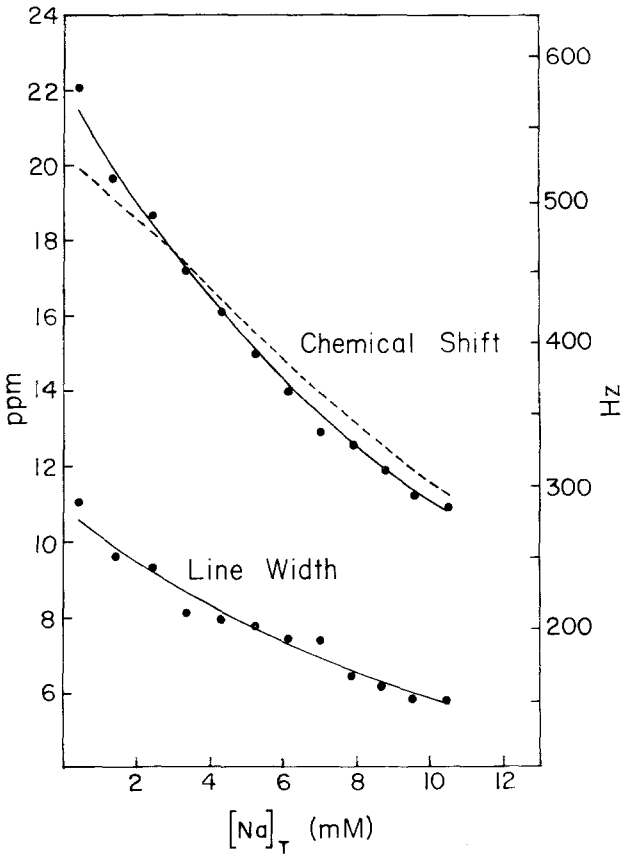

Fig. 3. Concentration dependence of chemical shift and line width, $C_T \sim 3$ mM. Solid curves are the theoretically calculated chemical shifts and line widths assuming one tight site per channel molecule. The chemical shift curve corresponds to $K_b^t = 146\,\text{M}^{-1}$ and $\nu_t = 1850$ Hz, while the line width fitting uses $K_b^t \sim 125\,\text{M}^{-1}$ and $\nu_{\frac{1}{2}}^t \sim 995$ Hz, ignoring the exchange term in Eq. (8). The broken line represents the least-squares minimized chemical shift, assuming two tight sites per channel molecule (as in the 4-site models) using $K_b^t = 290\,\text{M}^{-1}$ and $\nu_t = 825$ Hz. It may be seen that the assumption of one tight site per channel molecule is more consistent with the experimental data

at the tight site may be expected to be smaller if the exchange term in Eq. (8) were included.

It may be noted that the chemical shift and line width data, at low concentrations of 0.5–10 mM, show larger tight binding constants by a factor of two than obtained from analysis of the ELR plot. This may be an indication of the kind of precision with which the binding constants are obtained for the type of system under study. In this context it must be pointed out that besides NMR experimental limitations measuring chemical shift and line width accurately at low $[\text{Na}]_T$, there is also some variability in the micellar incorporation of malonyl gramicidin. Thus, repetition of the ion titration experiments with another preparation of the micellar incorporated channel molecules, resulted in some variation in the chemical shift and line width data. It is in this respect that it is very useful to consider the $\nu_{1/2}$ *vs.* ν plot.

4. Analysis of the Line Width *vs.* Chemical Shift Plot

A plot of the line width against the chemical shift is shown in Fig. 4. The experimental data points from four separate runs of the ion titration corresponding to various C_T are shown. Since the relation between $\nu_{1/2}$ and ν does not explicitly involve P_b, the fraction of the ions bound (*see* Eq. (9)), the shape of the $\nu_{1/2}$ *vs.* ν plot is independent of the binding constant and of the concentrations C_T and $[\text{Na}]_T$. In fact, the shape of this plot depends explicitly only on the three quantities ν_t, $\nu_{1/2}^t$ and k_{off}^t. Using the value of ν_t obtained from the chemical shift data, the values of $\nu_{1/2}^t$ and k_{off}^t are adjusted until the $\nu_{1/2}$ *vs.* ν plot calculated using Eq. (9) agree with experimental data points. Using ν_t of 1850 Hz obtained from the two- and three-site models, values of $\nu_{1/2}^t = 840 \pm 50$ Hz and $k_{\text{off}}^t = 10^{5\cdot5}$/sec (with an allowable range of 10^5 to $10^{6\cdot5}$) give the best fit to the data points. More general expressions valid for intermediate exchange (Eqs. (9)–(11) of Feeney et al., 1979) result in virtually identical values.

On fitting three sets of chemical shift data, the tight binding constant for one tight site/channel models varied from 100 to $146\,\text{M}^{-1}$ and, as was noted above, the ELR plots resulted in values of about $65\,\text{M}^{-1}$. Since binding one ion in the two-site model destroys two tight sites, this suggests a two-site model. For the single-channel current calculations a rounded mean number of $100\,\text{M}^{-1}$ will be used for K_b^t. For the weak site, K_b^w is $1\,\text{M}^{-1}$ for the two-site model and $0.5\,\text{M}^{-1}$ for the three-site models. The relevant values for the three occupancy models are given in Table 1.

B. Concentration and Voltage Dependence of Single-Channel Currents

The single-channel currents for malonyl gramicidin in diphytanoyl L-α-lecithin membranes are given in Fig. 5*A* as a function of concentration corrected to molal activities and for four different transmembrane potentials, 50, 100, 150, and 200 mV. The currents are approximately one-half the magnitude found for gramicidin channels in lecithin membranes (Kolb, Läuger & Bamberg, 1975; Bamberg, Kolb & Läuger, 1976; Anderson & Procopio, 1980). A lecithin membrane is favorable for comparison with studies on malonyl gramicidin incorporated into lysolecithin micelles because of the common polar head group and because it is likely that the barrier at the mouth of the channel is the rate limiting barrier. This is because the single-channel conductances vary with lipids containing different polar head groups, e.g., for

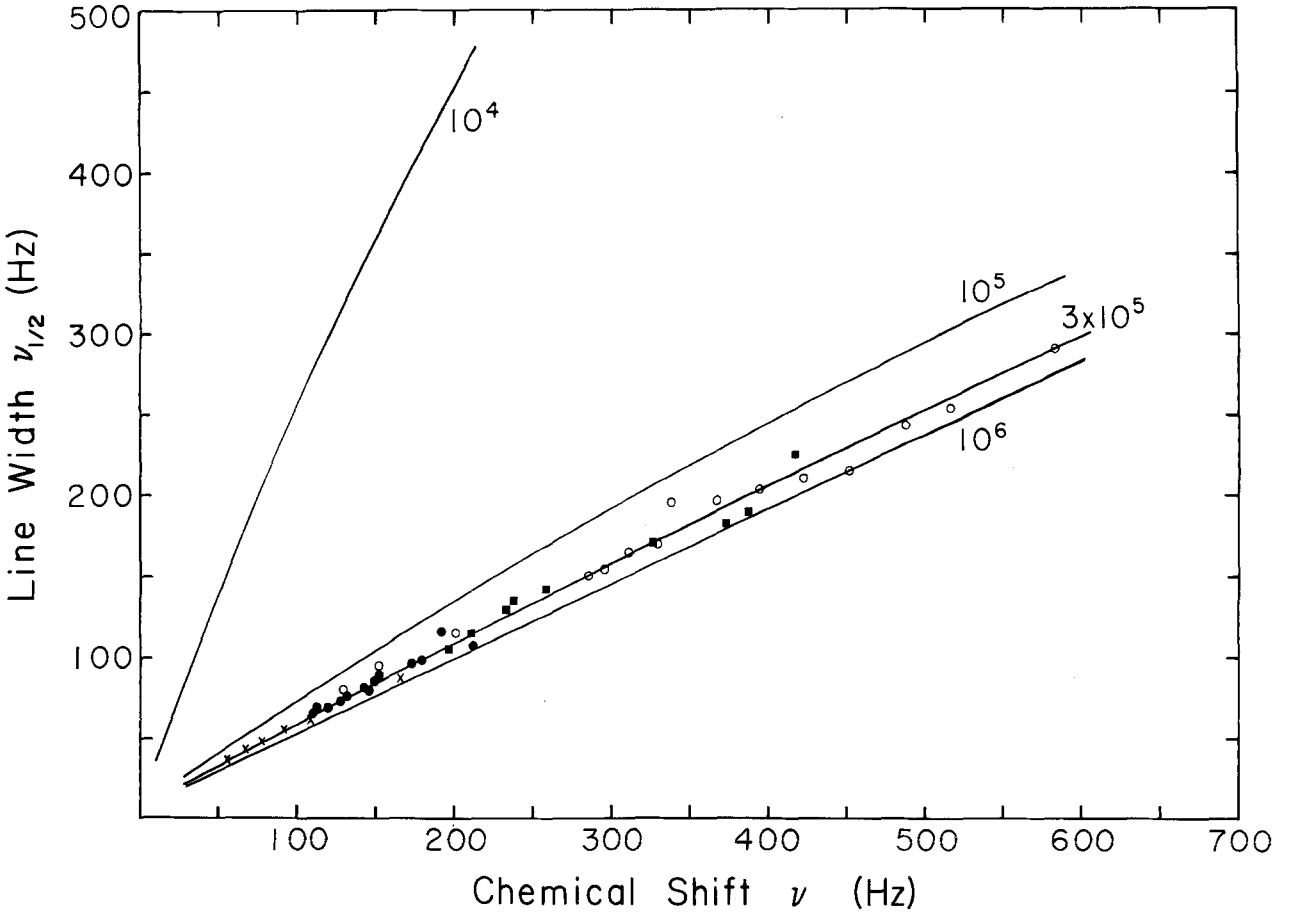

Fig. 4. A plot of the line width at half height, $\nu_{1/2}$ (in Hz) against chemical shift ν (in Hz). Experimental data points represent four separate runs of titrations using different micellar malonyl gramicidin preparations. The lines are theoretical calculated plots using general expressions valid for intermediate exchange (Feeney et al., 1979) using $\nu_t = 1{,}850$ Hz, $\nu^t_{1/2} = 838$ Hz for various values of k^t_{off}. The plot with $k^t_{off} = 3 \times 10^5$/sec agrees well with the experimental data

Table 1. NMR-derived binding and rate constants

	2-Site	3-Site	4-Site
K^t_b (M^{-1})	100	100	300
K^w_b (M^{-1})	1	0.5	0.5
K^t_{off} (sec^{-1})	3×10^5	3×10^5	2×10^5
k^w_{off} (sec^{-1})	2×10^7	2×10^7	2×10^7
k^t_{on} ($M^{-1}\,sec^{-1}$)	3×10^7	3×10^7	6×10^7
k^w_{on} ($M^{-1}\,sec^{-1}$)	2×10^7	1×10^7	1×10^7
k_{cb} or k_{cs} (sec^{-1})[a]	3.2×10^6	1.2×10^6[b]	1×10^9[c]

[a] Values obtained from least-square current fitting.
[b] This value applies to the virtual three-site model.
[c] Arbitrary maximal value used in calculations.

glyceryl monooleate membranes the conductance by gramicidin is about 25 pS (Hladky, Urban & Haydon, 1979), whereas for lecithin membranes it is about 11 pS at 25 °C, 1 M NaCl and 100 mV, because the two-site models of Hladky et al (1979) and of Anderson and Procopio (1980) give the major barrier at the mouth, because the barrier for the off-rate from the tight binding site at low concentration is the same as for transport through the channel (*see* the Introduction), and because, as will be seen below, the experimental currents of Fig. 5*A* can be reasonably calculated with the rate constants from the present nuclear magnetic resonance studies with two models which have the rate-limiting barrier at the mouth of the channel.

C. Calculation of Single-Channel Currents Using NMR-Derived Rate Constants

Given the steady-state schemes and steady-state equations of Appendix A, the values of the χ_i can be solved as indicated in Appendix B as a function of concentration and rate constants. Thus for the general current equation, or for the single-barrier current equation, there is now required the appropriate definition of rate constants and of distances and the introduction of voltage dependence. From the so-

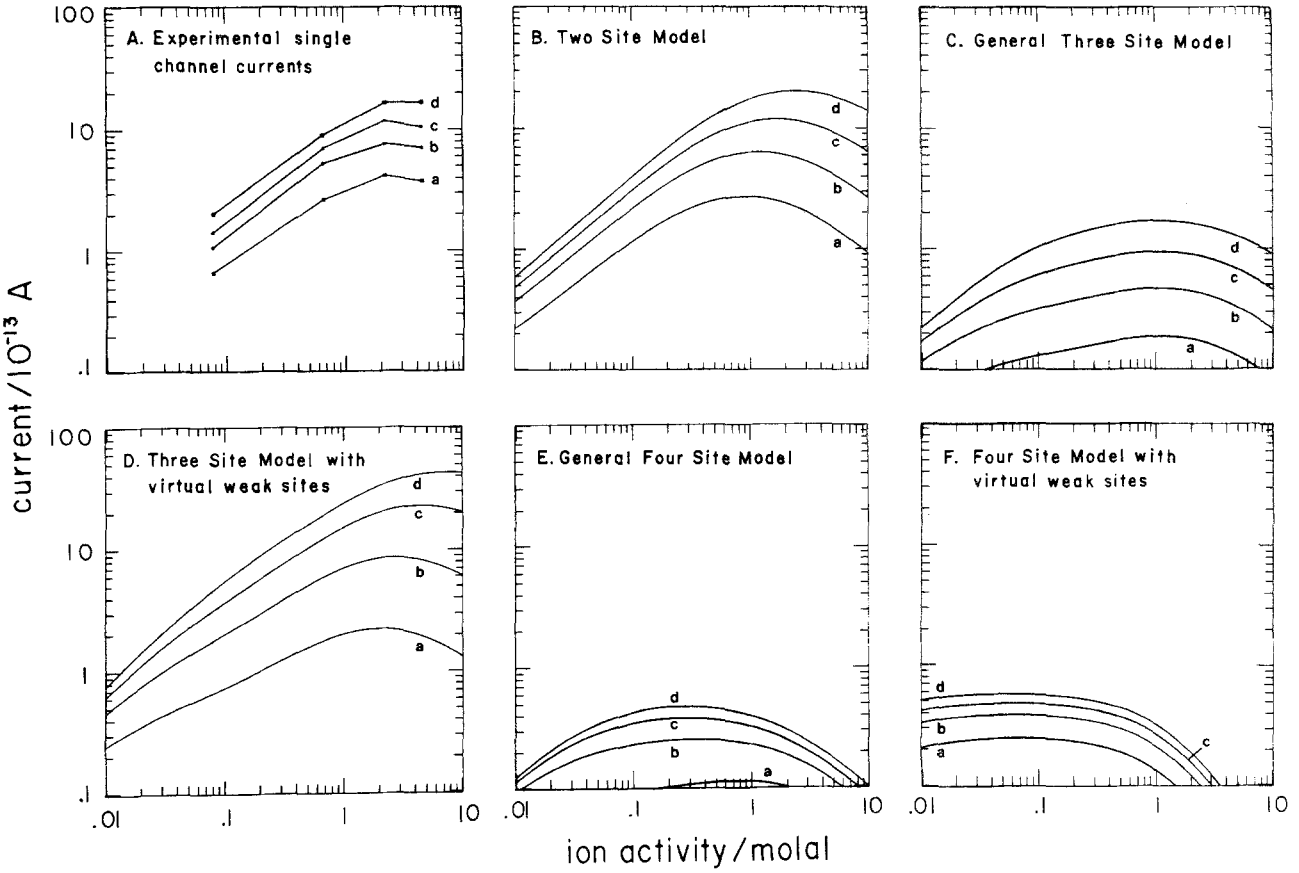

Fig. 5. Single-channel currents as a function of ion activity for various applied transmembrane voltages: (*a*) 50 mV, (*b*) 100 mV, (*c*) 150 mV, and (*d*) 200 mV. (*A*): Experimental data. (*B–F*): Theoretically calculated single-channel currents using rate constants derived from NMR data (*see* Table 1). Wherever applicable, the intrachannel translocation (k_{cb} for *B*, *E* and *F* and k_{sh} for *D*) was adjusted to obtain a least-squares fit of the currents with the experimental data in *A*. Such an optimization of k_{cb} was unsuccessful for the four-site models (*E* and *F*) and so these plots correspond to $k_{cb}=10^9$/sec. Note that the general three-site model in *C* contains no such adjustable parameter

dium-23 nuclear magnetic resonance data there are four rate constants defined (*see* Table 1) and there is a limited range placed on any intrachannel ion translocation in that the latter rate process must be slower than a diffusion controlled limit of 10^{10}/sec (Chock et al., 1977) and faster than k^t_{off}. Accordingly, with the NMR-derived rate constants, with the ion locations taken from the crystal structure studies, and with Eyring rate theory, there are all the quantities required to calculate with, at most, one parameter but that parameter must fall within a limited range.

1. The Two-Site Model – (General)

Using Fig. A-1*b* of Appendix A, lengths may be defined $\ell_1=(d-b_1)$, $\ell_2=(b_1-a_1)$ where $d=15$ Å, $a_1=10.5$ Å and $b_1=13$ Å. With the definition from the Methods section that $X\equiv\exp(zFE/2dRT)$ the desired voltage-dependent rate constants can be written as

$$k^1=k^t_{\text{on}}X^{\ell_1};\quad k^{-1}=k^t_{\text{off}}X^{-\ell_2};$$
$$k^2=k^t_{\text{off}}X^{\ell_2};\quad k^{-2}=k^t_{\text{on}}X^{-\ell_1};$$
$$k^3=k^w_{\text{off}}X^{\ell_2};\quad k^{-3}=k^w_{\text{on}}X^{-\ell_1};$$
$$k^4=k^w_{\text{on}}X^{\ell_1};\quad k^{-4}=k^w_{\text{off}}X^{\ell_2};$$
$$k^5=k_{cb}X^{a_1}\quad\text{and}\quad k^{-5}=k_{cb}X^{-a_1}$$

where $10^{10}>k_{cb}\geqq k^t_{\text{off}}$ is the range of values to which the rate constant for movement over the central barrier is restricted. With the values in Table 1 for the two-site model and using either Eqs. (A2), (A3) or (A4), the single-channel currents of Fig. 5*B* are calculated with $k_{cb}=3.2\times10^6$/sec.

2. The Three-Site Model – (General)

Using Fig. A-2*b* of Appendix A to define the lengths $\ell_1=(d-b_2)$, $\ell_2=(b_2-a_2)$ and $\ell_3=(a_2-b_1)$ where $d=15$ Å, $b_1=6.5$ Å, $b_2=13$ Å and $a_2=10.5$ Å, the volt-

age-dependent rate constants are written considering all weak sites as equal whether there are none, one, or two other ions in the channel, i.e.,

$k^1 = k^5 = k^8 = k^{12} = k^w_{on} X^{\ell_1}$;
$k^{-1} = k^{-5} = k^{-8} = k^{-12} = k^w_{off} X^{-\ell_2}$;
$k^2 = k^6 = k^7 = k^{11} = k^w_{off} X^{\ell_2}$;
$k^{-2} = k^{-6} = k^{-7} = k^{-11} = k^w_{on} X^{-\ell_1}$;
$k^3 = k^{10} = (k^t_{on}/K^w_b) X^{\ell_3}$;
$k^{-3} = k^{-10} = k^t_{off} X^{-b_1}$;
$k^4 = k^9 = k^t_{off} X^{b_1}$;
$k^{-4} = k^{-9} = (k^t_{on}/K^w_b) X^{-\ell_3}$.

In this model there is no parameter but there are the neglected ion repulsions noted above, and a doubly degenerate central site with 5 Å separation is treated as a single site. The calculated single-channel currents are given in Fig. 5*C*.

3. The Three-Site Model with Virtual Weak Sites

As will be considered in the Discussion section, should there be occupancy greater than two, the NMR data argues that a virtual weak site model is required where the weak site is formed after occupancy of the tight site. Using Fig. A-3*b* the lengths $\ell_1 = (d - b_2)$ and $\ell_2 = (b_2 - a_2)$ with $d = 15$ Å, $b_2 = 13$ Å, and $a_2 = 10.5$ Å are defined and the voltage-dependent rate constants are written:

$k^1 = k^t_{on} X^{\ell_1}$; $k^{-1} = k^t_{off} X^{-b_2}$;
$k^2 = k^t_{off} X^{b_2}$; $k^{-2} = k^t_{on} X^{-\ell_1}$;
$k^3 = k^7 = k^w_{on} X^{-\ell_2}$; $k^{-3} = k^{-7} = k^w_{off} X^{-\ell_2}$;
$k^4 = k^6 = k^w_{off} X^{\ell_2}$; $k^{-4} = k^{-6} = k^w_{on} X^{-\ell_1}$;
$k^5 = k_{cs} X^{2a_2}$ and $k^{-5} = k_{cs} X^{-2a_2}$

where the central shift of a pair of ions has the possible range of $10^{10} > k_{cs} \geqq k^t_{off}$. To be strictly in accord with the X-ray data the central tight site should be doubly degenerate and separated by 5 Å. For simplicity this is combined at a single central location. The weak sites are centered within the first outer turn of helix 2.5 Å from the carboxyl end. The calculated single-channel currents as a function of activity and voltage for this model are given in Fig. 5*D* and the value for k_{cs} is 1.2×10^6/sec.

4. The Four-Site Model – (General)

With reference to Fig. A-4*b* and as with the two-site model, the X-ray data places the tight site at 10.5 Å (a_1) from the center and the NMR data argues that the weak site is an outer site (*see* Discussion below). Accordingly, b_1 is still taken at 13 Å and a_2 is at 15 Å with b_2 beyond the length over which the potential drop is taken such that d and b_2 are both taken at 15 Å. Defining the lengths, in general, as $\ell_1 = (d - b_2)$, $\ell_2 = (b_2 - a_2)$, $\ell_3 = (a_2 - b_1)$ and $\ell_4 = (b_1 - a_1)$, the voltage-dependent rate constants are written for those ion movements with the potential gradient as,

$k^1 = k^7 = k^9 = k^{11} = k^{20} = k^{21} = k^{25} = k^{28} = k^w_{on} X^{\ell_1}$;
$k^2 = k^6 = k^8 = k^{10} = k^{18} = k^{19} = k^{26} = k^{27} = k^w_{off} X^{\ell_2}$;
$k^3 = k^{14} = k^{16} = k^{22} = (k^t_{on}/K^w_b) X^{\ell_3}$;
$k^5 = k^{13} = k^{17} = k^{24} = k^t_{off} X^{\ell_4}$;
$k^4 = k^{12} = k^{15} = k^{23} = k_{cb} X^{a_1}$.

The other half of the rate constants for movement up the potential gradient can be written by symmetry and by comparison with the simpler models. As seen in Fig. 5*E*, this model does not give very satisfactory values for single-channel currents. This may, of course, be due to the neglect of certain ion-ion repulsions. The interactions of ions in positions 1 and 2 with 3 and 4 are neglected; the interaction between 1 and 2 and between 3 and 4 are considered to occur in the determined rate and binding constants, and the binding at sites 1 and 4 are taken to be the same whether or not sites 2 or 3 are occupied. Admittedly these are gross assumptions, but it is of particular interest to demonstrate that given the one adjustable value of k_{cb}, the experimental currents cannot be approached. As will be seen below, even with a virtual weak site-four site model which adheres better to the dictates of the NMR studies and which only neglects the ion interactions at 21 Å or greater, the comparison of calculated with experimental values fares no better.

5. *The Four-Site Model with Virtual Weak Sites*

In the virtual weak site-four site model, depicted in Fig. A-5, the weak site is considered not to be stable until its paired tight site is filled and improbable simultaneous two-ion jumps are not considered. Defining the lengths $\ell_1 = (d - b_2)$, $\ell_2 = (b_2 - a_2)$ and $\ell_3 = (b_2 - a_1)$, the voltage-dependent rate constants are written

$k^1 = k^6 = k^8 = k^t_{on} X^{\ell_1}$; $k^{-1} = k^{-6} = k^{-8} = k^t_{off} X^{-\ell_3}$;
$k^2 = k^5 = k^7 = k^t_{off} X^{\ell_3}$; $k^{-2} = k^{-5} = k^{-7} = k^t_{on} X^{-\ell_1}$;
$k^3 = k^9 = k^{12} = k^w_{on} X^{\ell_1}$; $k^{-3} = k^{-9} = k^{-12} = k^w_{off} X^{-\ell_2}$;
$k^4 = k^{10} = k^{11} = k^w_{off} X^{\ell_2}$; $k^{-4} = k^{-10} = k^{-11} = k^w_{on} X^{-\ell_1}$;
$k^{13} = k_{cb} X^{2a_1}$ and $k^{-13} = k_{cb} X^{-2a_1}$

where the lengths are the same as for the general four-site model. The calculated single-channel currents are given in Fig. 5*F*. This model which retains a

certain consistency with the NMR data and which does not have a serious neglect of ion-ion interactions is not capable of approaching the experimental values. The treatment does neglect ion repulsion occurring at 21 Å or more, but this is not serious for a model which necessarily states that a second ion can bind within 5 Å of an initial ion with less than a 10^2 difference in binding constant and at a site which is inherently weaker, whereas the same neglect of ion-ion interactions at 21 Å in the virtual three-site model does give rise to reasonable currents.

Discussion

General Requirements of the Energy Profile

At low concentrations, 1–10 mM, the temperature dependence of line width (Urry et al., 1979*a–b*) and of T_1 (*see* Fig. 6) give an activation energy for exchange with the channel of 7.2 ± 0.2 kcal/mole whereas the activation energy for transport through the channel is reported as 7.3 kcal/mole (Bamberg & Läuger, 1974). This result is interpreted to require that no barrier in traversing the channel is higher than the barrier encountered on passing from solution to the tight site. All of the models considered here adhere to that requirement of the energy profile (*see* the five figures of Appendix A).

Since at high concentrations a weak site is observed in which the ion exchanges between solution and a channel interaction site, for a single-filing channel this requires that the weak site be external to the tight site; for if the weak site were central to the tight site, the ion movement from solution to the weak site would require passing over the major barrier through the tight site to the weak site in which case the major barrier would allow only a slower exchange between solution and channel. Thus in all the models considered here, the weak site is located external to the tight site, or more correctly to include the two-site model, the weak site is reached without passing through the tight site.

There is yet another restriction on the energy profiles; that is the positioning of the major barrier with respect to the weak and tight sites. If the major barrier were located between the weak and tight sites as in Figs. 9 and 11 for the general three- and four-site models, then the ion in solution should be able to exchange many times between solution and the weak site during the time for a single exchange between solution and the tight site. This means that the relaxation properties of the pool of ions would be dominated by the weak site even at relatively low concentrations even though the binding constant at low concentration as determined from the chemical shift data would reflect the free energy change on going to the tight site. There may be a suggestion of this effect since the binding constant determined by fitting the chemical shift *vs.* ion concentration data (*see* Fig. 3) at low concentration results in a value which is greater by a factor of two than that obtained from fitting of the ELR plot of Fig. 2*A*. While we believe that this factor of two is within the error for estimating such binding constants, it may be a reflection of the statistics for a two-site model.

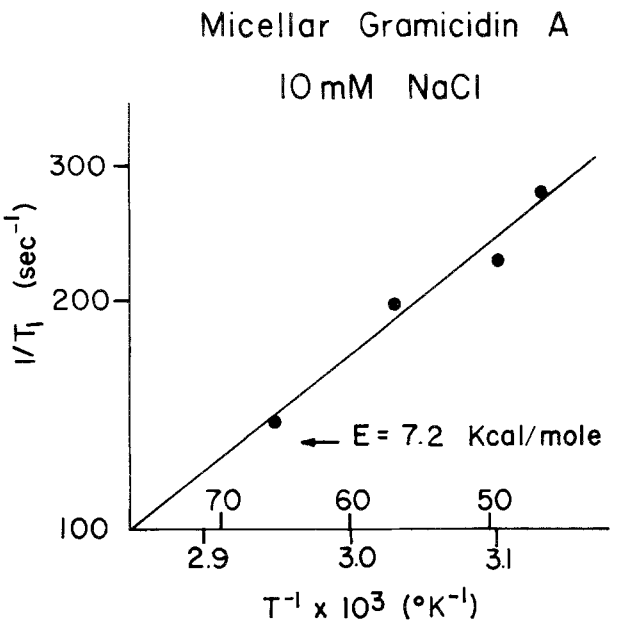

Fig. 6. Temperature dependence of the longitudinal relaxation time, T_1, giving an energy of activation of 7.2 kcal/mole for exchange of Na^+ with the channel, realizing that $1/T_1$ is directly proportional to $\tau_c [= A \exp(E/RT)]$

The implication, that the relaxation properties are determined by the off rate from the tight site ($k^t_{off} \simeq 3 \times 10^5$/sec) at low concentration, however, is that the weak site is a virtual site which occurs only after the channel has been occupied at a tight site. This is the case whether the model is the general two-site or one of the virtual three- and four-site models. In the two-site model, while the weak site occurs at the location of a possible tight site for one ion in the channel, the repulsion between ions on entry of the second ion creates two weak sites. In the virtual three- and four-site models, on the other hand, the second ion has passed over the major barrier and cannot slide energetically down hill into the tight site as it is occupied. The energy barrier on one side and the repulsion from the ion in the tight site on the other side creates or stabilizes a weak binding site.

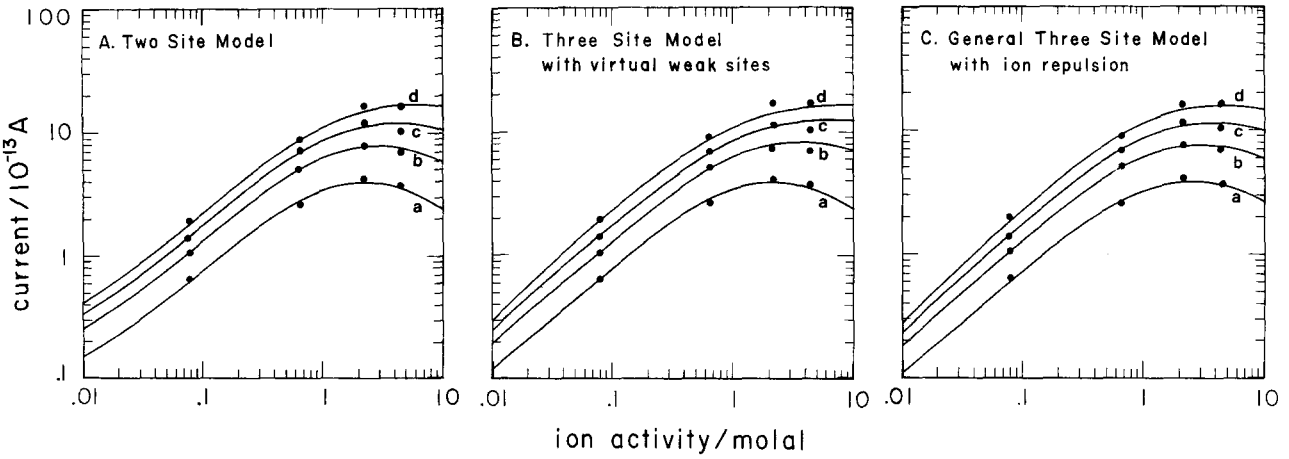

Fig. 7. Single-channel currents least-squares fitted to the experimental data. All rate constants have been adjusted to produce an optimum fitting with the experimentally measured current for various ion concentrations and transmembrane potentials: (*a*) 50 mV, (*b*) 100 mV, (*c*) 150 mV, and (*d*) 200 mV. The following values have been used in calculating the currents:

A) $K_b^t = 200\,\mathrm{M}^{-1}$, $K_b^w = 1.3\,\mathrm{M}^{-1}$, $k_{\mathrm{off}}^t = 1.6 \times 10^5\,\mathrm{sec}^{-1}$, $k_{\mathrm{off}}^w = 7.9 \times 10^6\,\mathrm{sec}^{-1}$, $k_{cb} = 1.3 \times 10^7\,\mathrm{sec}^{-1}$.
B) $K_b^t = 100\,\mathrm{M}^{-1}$, $K_b^w = 1.0\,\mathrm{M}^{-1}$, $k_{\mathrm{off}}^t = 1.1 \times 10^5\,\mathrm{sec}^{-1}$, $k_{\mathrm{off}}^w = 5.8 \times 10^6\,\mathrm{sec}^{-1}$, $k_{cs} = 4.8 \times 10^6\,\mathrm{sec}^{-1}$.
C) $K_b^t = 75\,\mathrm{M}^{-1}$, $K_b^w = 1.0\,\mathrm{M}^{-1}$, $k_{\mathrm{off}}^t = 2.9 \times 10^7\,\mathrm{sec}^{-1}$, $k_{\mathrm{off}}^w = 7.2 \times 10^6\,\mathrm{sec}^{-1}$ and $A = 3.1$ kcal-Å/mole

Comparison of Experimental and Calculated Single-Channel Currents

In Fig. 5, it is apparent that the two-site and the virtual three-site models result in very reasonable currents whereas the general three-site and four-site models do not. Since the neglect of ion-ion repulsions at 21 Å is common to both the virtual three-site and the virtual four-site models, the inability of the four-site models to derive reasonable currents, using the NMR-derived rate constants, casts doubt on the four-site models considered. This is consistent with efforts to calculate the chemical shift data of Fig. 3 which indicated a poor fit of the data when assuming two tight binding sites per malonyl gramicidin molecule (i.e., per channel).

Recognizing that the error in the magnitude of the NMR-derived constants can be a factor of two and is likely more, it is of interest to determine how well the single-channel currents could be calculated by allowing the magnitude of the four experimentally derived constants to vary. The results of this are given in Fig. 7*A* and *B* where the calculated currents for the two-site and virtual three-site models can be found to fit extraordinarily well over the entire concentration range and for each of the four voltages used. While the best estimates of the experimental constants were

$$K_b^t = 100\,\mathrm{M}^{-1}, \quad K_b^w = 1\,\mathrm{M}^{-1}, \quad k_{\mathrm{off}}^t = 3 \times 10^5/\mathrm{sec}$$

and

$$k_{\mathrm{off}}^w = 2 \times 10^7/\mathrm{sec},$$

the best fit values change only to

$$K_b^t = 200\,\mathrm{M}^{-1}, \quad K_b^w = 1.3\,\mathrm{M}^{-1}, \quad k_{\mathrm{off}}^t = 1.6 \times 10^5/\mathrm{sec}$$

and $k_{\mathrm{off}}^w = 0.79 \times 10^7/\mathrm{sec}$ for the two-site model and to

$$K_b^t = 100\,\mathrm{M}^{-1}, \quad K_b^w = 1\,\mathrm{M}^{-1}, \quad k_{\mathrm{off}}^t = 1.1 \times 10^5/\mathrm{sec}$$

and $k_{\mathrm{off}}^w = 0.58 \times 10^7/\mathrm{sec}$ for the virtual three-site model. Thus by letting the constants change to obtain a best fit, the new values differ by no more than about a factor of two, i.e., within experimental limits. This is compelling evidence for the utility of NMR in the study of ion channel interactions and for the potential credibility of the two models.

The above does not imply, however, that other models are not capable of fitting the current curves with constants other than those derived from the NMR data. If, for example, the values of all four constants of the general three-site model are allowed to vary, a good fit can be achieved, but k_{off}^t is found to change by almost two orders of magnitude to $2.1 \times 10^7/\mathrm{sec}$ with the other values exhibiting smaller changes, i.e.,

$$K_b^t = 75\,\mathrm{M}^{-1}, \quad K_b^w = 1\,\mathrm{M}^{-1},$$

and

$$k_{\mathrm{off}}^w = 0.78 \times 10^7/\mathrm{sec}.$$

This demonstrates, therefore, how crucial it is to have independent determinations of the required constants because there is not a unique set of four or five constants that are required to calculate the single-

channel currents as a function of voltage and concentration.

Introduction of Ion-Ion Repulsion. A good fit of the general three-site model to the single-channel currents was achieved by four parameters whereas five were used in Fig. 7*A* and *B*. It is instructive to include the neglected ion-ion interactions as a fifth parameter in the general three-site model, by considering the repulsion to have an r^{-1} distance dependence and taking the effective dielectric constant to be constant for distances of 10.5 Å and larger. The new definitions of voltage-dependent rate constants become:

$$k^1 = k^w_{on} X^{\ell_1} \exp(\alpha'/RT);$$
$$k^{-1} = k^w_{off} X^{-\ell_2} \exp[(\alpha' - \alpha)/RT];$$
$$k^2 = k^w_{off} X^{\ell_2} \exp[(\alpha' - \alpha)/RT];$$
$$k^7 = k^w_{off} X^{\ell_2} \exp[(\alpha''' - \alpha'')/RT];$$
$$k^{-7} = k^w_{on} X^{-\ell_1} \exp(\alpha'''/\mathrm{RT});$$
$$k^8 = k^w_{on} X^{\ell_1} \exp(\alpha'''/RT);$$
$$k^{-8} = k^w_{off} X^{-\ell_2} \exp[(\alpha''' - \alpha'')/RT];$$
$$k^9 = k^t_{off} X^{b_1} \exp[(\alpha - \alpha^{iv})/RT];$$
$$k^{-9} = (k^t_{on}/K^w_b) X^{-\ell_3} \exp(\alpha^{iv}/RT);$$
$$k^{10} = (k^t_{on}/K^w_b) X^{\ell_3} \exp(\alpha^{iv}/RT);$$
$$k^{-10} = k^t_{off} X^{-b_1} \exp[(\alpha - \alpha^{iv})/RT];$$
$$k^{11} = k^w_{off} X^{\ell_2} \exp[-(\alpha''' - \alpha'')/RT];$$
$$k^{-11} = k^w_{on} X^{-\ell_1} \exp(-\alpha'''/RT);$$
$$k^{12} = k^w_{on} X^{\ell_1} \exp(-\alpha'''/RT);$$
$$k^{-12} = k^w_{off} X^{-\ell_2} \exp[-(\alpha''' - \alpha'')/RT],$$

and the other rate constants are as previously defined for the general three-site model. The α are defined as $\alpha = A/a_2$; $\alpha' = A/b_2$; $\alpha'' = A/2a_2$; $\alpha''' = A/(a_2 + b_2)$ and $\alpha^{iv} = A/(a_2 + b_1)$. The new parameter, A, is a repulsion energy times length in Angstroms. As may be seen in Fig. 7*C*, an excellent fit is obtained with $K^t_b = 75\ \mathrm{M}^{-1}$; $K^w_b = 1\ \mathrm{M}^{-1}$, $k^t_{off} = 2.9 \times 10^7$/sec, $k^w_{off} = 0.72 \times 10^7$/sec and $A = 3.1$ kcal − Å/mole. If this model were correct, one would conclude that the repulsion between monovalent sodium ions separated by 10.5 Å would be only 0.3 kcal/mole. This model, however, is not to be concluded as correct. It is presented here for the purpose of demonstrating a general procedure for introducing ion-ion repulsion and it is done with the general three-site model, as it can be achieved with the same number of parameters as used with the other models. On the other hand, if the two-site model were correct, then the difference between the two binding constants would provide the value for A, i.e., $K^w_b = \exp(-\alpha/RT)\ K^t_b$. With $K^w_b = 1$ and $K^t_b = 100$ and $\alpha = A/21$, the value for A becomes 58 kcal − Å/mole. Our lack of knowledge of the true repulsion energy is exemplified by the two values obtained for A, i.e., 3 and 58. Yet another estimate of A is obtained from the virtual three-site model where it could be argued that $k^t_{on} = k^w_{on} \exp(\alpha/RT)$ where $\alpha = A/b_2$ such that $A = 4.5$ kcal · Å/mole. By the same analysis for the two-site model, A is negative. This latter apparent inconsistency of the two-site model has been discussed elsewhere (Urry et al., 1980). Consideration of the general three-site model and the four-site models imply that values of the order of 3 kcal · Å/mole are reasonable, whereas for a two-site model to be correct the value would be about 60 kcal · Å/mole. The difference of a factor of 20 emphasizes how poorly this important quantity is known. It is, of course, of primary importance that the positions of the weak and tight sites within the channel be experimentally determined after which the correct model can be chosen and a correct value of A estimated.

The experimental positioning of the ions within the channel will determine whether the two- or the virtual three-site model is correct, which will allow, with the NMR-derived rate constants, a complete description of sodium transport through the gramicidin channel, including an evaluation of the fundamental value for monovalent cation-monovalent cation repulsion under conditions of complexation in the channel.

The authors wish to acknowledge the National Institutes of Health Grant Nos. GM-26898 and GM-07195; the Konstanz group, E. Bamberg, H.-A. Kolb, H.J. Apell and particularly P. Läuger for many informative and stimulating discussions, and Md. A. Khaled of this Laboratory for his contributions to the early phases of the NMR work.

Appendix A

Multiple Occupancy Models: Steady-State Equations, Single Channel Current Equations and Schematic Energy Profiles

The sodium-23 nuclear magnetic resonance data on micellar-packaged gramicidin (Urry et al., 1980) and malonyl gramicidin (presented above) demonstrate two resolvable binding constants, representing a tight site and a weak site, and the crystal structure studies on gramicidin cation complexes of the Stryer group (Koeppe et al., 1979) demonstrate two occupiable sites which by comparison with the NMR data would be possible tight binding sites. While the crystal structure data do not demonstrate simultaneous occupancy (i.e., multiple occupancy) within a single 26-Å length of channel, the sodium-23 nuclear magnetic resonance data do indicate a second binding site, i.e., a second ion occupancy, becoming significant at concentrations of 100 mM and above. Accordingly, mul-

tiple occupancy models are required from these studies which, in fact, confirm previous deductions from electrical measurements on gramicidin-doped lipid bilayers (Eisenman, Sandblom & Neher, 1977; Sandblom et al., 1977; Eisenman, Sandblom & Neher, 1978; Urban, Hladky & Haydon, 1978; Hägglund, Enos & Eisenman, 1979; Hladky et al., 1979). Five single filing, multiple occupancy models are considered here in terms of steady-state schemes, steady-state equations, schematic energy profiles and single-channel currents.

Fundamental constraints imposed by the gramicidin channel structure are the twofold symmetry axis perpendicular to the helix (channel) axis and the channel diameter which allows only single filing of ion and water molecules over the 26-Å length of the channel. Possible positions for the tight binding sites are taken from the crystal structure data (Koeppe et al., 1979). Fundamental questions, which will be approached without prejudice, are the contribution to a central barrier of the positive image force due to the lipid of the lipid bilayer (Urry, 1978) and the repulsive force between ions within the channel. This initial, intentional lack of prejudice allows, for example, consideration of both a two-site model with a central barrier and with substantial repulsion at large distances (21 Å) and a three-site model with the most energetically favored position at the center midway through the channel, with modest repulsion at 10 Å and with neglected repulsion at 21 Å. These are conditions variously allowed or imposed by the physical data, depending on the occupancy model being considered.

1. The Two-Site Model — (General)

Because of the twofold symmetry of the gramicidin channel, the basic requirement of a two-site model is that the sites be identical and that the difference in binding between the first and second ion be due to repulsion. The tight binding site, therefore, is a case of single occupancy. Addition of a second ion to the channel results in there being two weakly bound ions in the channel. While the above are the structural dictates of the gramicidin channel, the steady-state schemes (*see* Fig. A-1*a*) and the following steady-state equations can be considered as general for a two-site model.

Two Site Model
(general)

1 a
Steady State Scheme

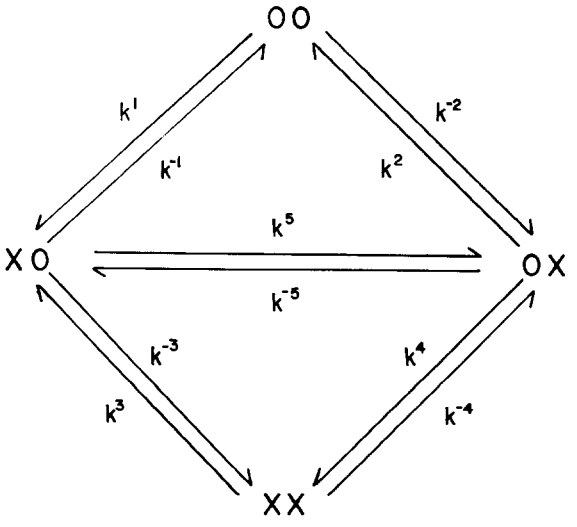

1 b
Energy Profile

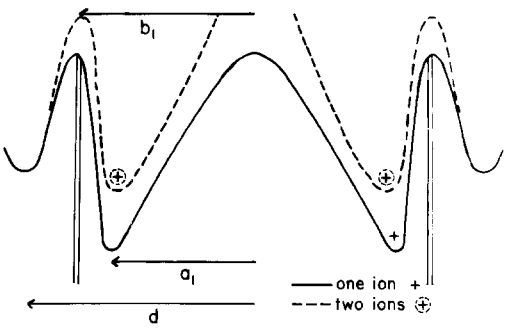

$$\dot{\chi}(o\,o) = -(C'_x k^1 + C''_x k^{-2})\chi(o\,o) + k^{-1}\chi(x\,o) + k^2\chi(o\,x) = 0 \quad (A1a)$$

$$\dot{\chi}(x\,o) = C'_x k^1 \chi(o\,o) - (k^{-1} + k^5 + C''_x k^{-3})\chi(x\,o) + k^{-5}\chi(o\,x) + k^3\chi(x\,x) = 0 \quad (A1b)$$

$$\dot{\chi}(o\,x) = C''_x k^{-2}\chi(o\,o) + k^5\chi(x\,o) - (k^2 + k^{-5} + C'_x k^4)\chi(o\,x) + k^{-4}\chi(x\,x) = 0 \quad (A1c)$$

$$\dot{\chi}(x\,x) = C''_x k^{-3}\chi(x\,o) + C'_x k^4\chi(o\,x) - (k^3 + k^{-4})\chi(x\,x) = 0$$

where the χ are the probabilities of the occupancy states, e.g., $\chi(o\,o)$ is the probability of the unoccupied channel; C'_x and C''_x are the concentrations (activities) of ion x on the positive (left-hand) side and the negative (right-hand) side of the membrane, respectively; the k^i are the constants for ion movements to the right and k^{-i} are for ion movements to the left as defined in the steady-state scheme (Fig. A-1 *a*) and the $\dot{\chi}$ are the changes in probabilities with time, i.e., the time derivatives, which under conditions of steady state are zero.

Given the lengths a_1, b_1 and d defined in the schematic energy profile for the transmembrane movement of the ion (*see* Fig. A-1 *b*), the general single-channel current equation can be written

$$I_x = \frac{z\,e}{2d}\{(d-a_1)(C'_x k^1 - C''_x k^{-2})\chi(o\,o) + [2a_1 k^5 - (d-a_1)(k^{-1} + C''_x k^{-3})]\chi(x\,o) + [(d-a_1)(k^2 + C'_x k^4) - 2a_1 k^{-5}]\chi(o\,x) + (d-a_1)(k^3 - k^{-4})\chi(x\,x)\} \quad (A2)$$

where z is the formal charge on the ion, e is the number of coulombs for a single charge and $2d$ is the total length over which the transmembrane potential is applied. This equation, however, is more complex than is required since, under steady-state conditions, it is necessary only to count the ions passing over a single barrier. When considering the left-hand barrier in Fig. A-1 *b*, the single-channel current becomes

$$I_x = z\,e[C'_x k^1 \chi(o\,o) - k^{-1}\chi(x\,o) + C'_x k^4\chi(o\,x) - k^{-4}\chi(x\,x)]. \quad (A3)$$

The identical single-channel current at steady state is even more simple when considering the central barrier, i.e.,

$$I_x = z\,e[k^5\chi(x\,o) - k^{-5}\chi(o\,x)]. \quad (A4)$$

It should be appreciated with Eq. (A4) that, while only the rate constants k^5 and k^{-5} are explicitly seen in this current equation, the other rate constants have their effect in determining the values for $\chi(x\,o)$ and $\chi(o\,x)$. Similarly, in Eq. (A3) the missing rate constants exert their effect in the values for the probabilities, or fraction of time, of each occupancy state. While Eqs. (A3) and (A4) do not contain lengths, the distances from binding site to rate limiting barrier are required for correct introduction of the voltage dependence (*see* Method section).

2. *The Three-Site Model – (General)*

The steady-state scheme for a general, single-filing, three-site channel model is given in Fig. A-2 *a* and the corresponding steady-state equations are the following,

$$\dot{\chi}(o\,o\,o) = -[C'_x k^1 + C''_x k^{-2}]\chi(o\,o\,o) + k^{-1}\chi(x\,o\,o) + k^2\chi(o\,o\,x) = 0 \quad (A5a)$$

$$\dot{\chi}(x\,o\,o) = -[k^{-1} + k^3 + C''_x k^{-7}]\chi(x\,o\,o) + C'_x k^1\chi(o\,o\,o) + k^{-3}\chi(o\,x\,o) + k^7\chi(x\,o\,x) = 0 \quad (A5b)$$

$$\dot{\chi}(o\,o\,x) = -[k^2 + k^{-4} + C'_x k^8]\chi(o\,o\,x) + C''_x k^{-2}\chi(o\,o\,o) + k^4\chi(o\,x\,o) + k^{-8}\chi(x\,o\,x) = 0 \quad (A5c)$$

$$\dot{\chi}(o\,x\,o) = -[k^{-3} + k^4 + C'_x k^5 + C''_x k^{-6}]\chi(o\,x\,o) + k^3 x(x\,o\,o) + k^{-4}\chi(o\,o\,x) + k^{-5}\chi(x\,x\,o) + k^6\chi(o\,x\,x) = 0 \quad (A5d)$$

$$\dot{\chi}(x\,o\,x) = -[k^7 + k^{-8} + k^{-9} + k^{10}]\chi(x\,o\,x) + C''_x k^{-7}\chi(x\,o\,o) + C'_x k^8\chi(o\,o\,x) + k^9\chi(x\,x\,o) + k^{-10}\chi(o\,x\,x) = 0 \quad (A5e)$$

$$\dot{\chi}(x\,x\,o) = -[k^{-5} + k^9 + C''_x k^{-11}]\chi(x\,x\,o) + C'_x k^5 \cdot\chi(o\,x\,o) + k^{-9}\chi(x\,o\,x) + k^{11}\chi(x\,x\,x) = 0 \quad (A5f)$$

$$\dot{\chi}(o\,x\,x) = -[k^6 + k^{-10} + C'_x k^{12}]\chi(o\,x\,x) + C''_x k^{-6}\chi(o\,x\,o) + k^{10}\chi(x\,o\,x) + k^{-12}\chi(x\,x\,x) = 0 \quad (A5g)$$

$$\dot{\chi}(x\,x\,x) = -[k^{11} + k^{-12}]\chi(x\,x\,x) + C''_x k^{-11}\chi(x\,x\,o) + C'_x k^{12}\chi(o\,x\,x) = 0. \quad (A5h)$$

The above equations are general and do not require a symmetrical placing of sites, but for application to the gramicidin channel twofold symmetry is imposed in the energy profile as indicated in Fig. A-2 *b*. When writing a general current equation as in Eq. A2, the lengths in Fig. A-2 *b* would be used and, as noted before, these lengths are required for the voltage dependence of the rate constants. An example of one of the four possible steady-state single-channel current equations written with respect to a selected

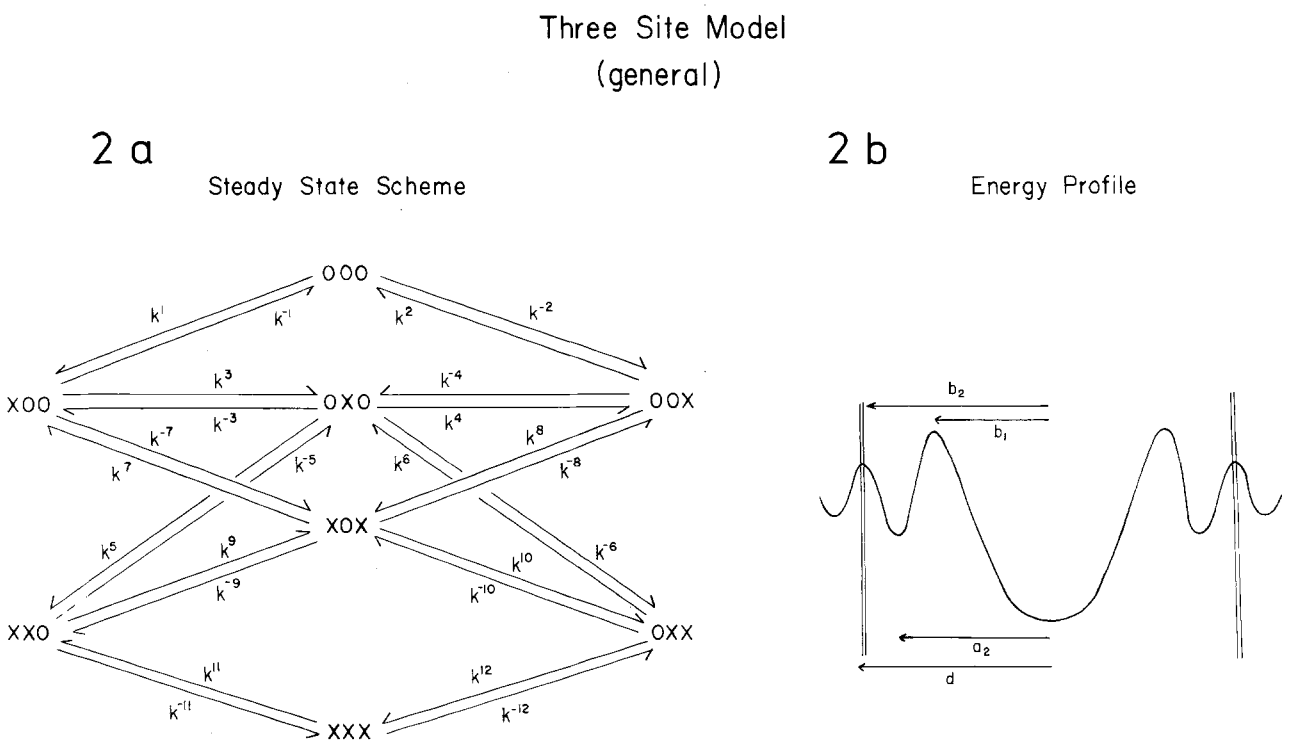

barrier, i.e., for the highest barrier on the left-hand side, becomes

$$I_x = z e[k^3 \chi(x\,o\,o) - k^{-3} \chi(o\,x\,o) + k^{10} \chi(o\,o\,x) - k^{-10} \chi(o\,x\,x)]. \quad \text{(A6)}$$

3. *The Three-Site Model with Virtual Weak Sites*

An additional type of single-filing, three-site model requires consideration due to the nuclear magnetic resonance data. This is a virtual weak site model where a central tight binding site fills first at low concentration and creates weak binding sites. Outer metastable sites, which would not have significant occupancy when a single ion traverses the channel, become sites due to the presence of an ion in the central site. The steady-state scheme for this model is given in Fig. A-3 with a schematic energy profile. The steady-state equations for the virtual weak-site three-site model are

$$\dot{\chi}(o\,o\,o) = -(C'_x k^1 + C''_x k^{-2}) \chi(o\,o\,o) + (k^{-1} + k^2) \chi(o\,x\,o) = 0 \quad \text{(A7a)}$$

$$\dot{\chi}(o\,x\,o) = (C'_x k^1 + C''_x k^{-2}) \chi(o\,o\,o) - (k^{-1} + k^2 + C'_x k^3 + C''_x k^{-4}) \chi(o\,x\,o) + k^{-3} \chi(x\,x\,o) + k^4 \chi(o\,x\,x) = 0 \quad \text{(A7b)}$$

$$\dot{\chi}(x\,x\,o) = C'_x k^3 \chi(o\,x\,o) - (k^{-3} + C''_x k^{-6} + k^5) \chi(x\,x\,o) + k^{-5} \chi(o\,x\,x) + k^6 \chi(x\,x\,x) = 0 \quad \text{(A7c)}$$

$$\dot{\chi}(o\,x\,x) = C''_x k^{-4} \chi(o\,x\,o) + k^5 \chi(x\,x\,o) - (k^4 + k^{-5} + C'_x k^7) \chi(o\,x\,x) + k^{-7} \chi(x\,x\,x) = 0 \quad \text{(A7d)}$$

$$\dot{\chi}(x\,x\,x) = C''_x k^{-6} \chi(x\,x\,o) + C'_x k^7 \chi(o\,x\,x) - (k^6 + k^{-7}) \chi(x\,x\,x) = 0 \quad \text{(A7e)}$$

and the general single-channel current equation is

$$I_x = \frac{z e}{2d} \{[dk^2 - dk^{-1}] \chi(o\,x\,o) + [2a_2 k^5 - (d - a_2) k^{-3}] \chi(x\,x\,o) + [(d - a_2) k^4 - 2a_2 k^{-5}] \chi(o\,x\,x) + [(d - a_2) k^6 - (d - a_2) k^{-7}] \chi(x\,x\,x) + C'_x d k^1 \chi(o\,o\,o) + C'_x (d - a_2) k^3 \chi(o\,x\,o) + C'_x (d - a_2) k^7 \chi(o\,x\,x) - C''_x d k^{-2} \chi(o\,o\,o) - C''_x (d - a_2) k^{-4} \chi(o\,x\,o) - C''_x (d - a_2) k^{-6} \chi(x\,x\,o)\}. \quad \text{(A8)}$$

The single-channel current at steady state and written for the left barrier becomes

$$I_x = z e[C'_x k^1 \chi(o\,o\,o) - k^{-1} \chi(o\,x\,o) + C'_x k^3 \chi(o\,x\,o) - k^{-3} \chi(x\,x\,o) + C'_x k^7 \chi(o\,x\,x) - k^{-7} \chi(x\,x\,x)]. \quad \text{(A9)}$$

Three Site Model
(virtual weak binding sites)

3 a
Steady State Scheme

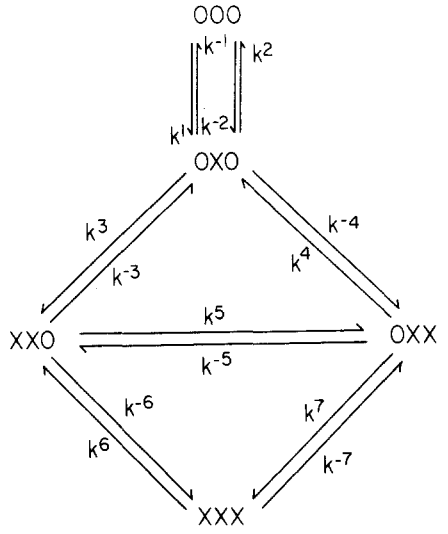

3 b
Energy Profile

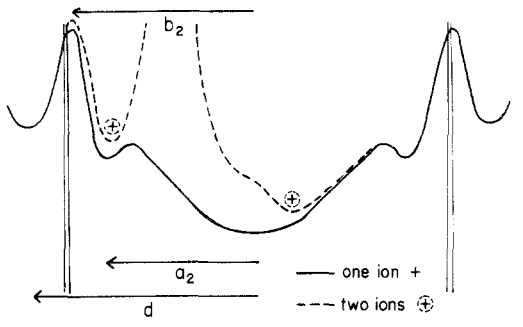

4. The Four Site Model – (General)

The general, single-filing, four-site model is characterized by sixteen states and 56 rate constants. The steady-state scheme and a corresponding schematic energy profile are given in Fig. A-4. The set of sixteen steady state equations are the following:

$$\dot{\chi}(oooo) = -(C'_x k^1 + C''_x k^{-2})\chi(oooo) + k^{-1}\chi(xooo) + k^2\chi(ooox) = 0 \quad (A10a)$$

$$\dot{\chi}(xooo) = C'_x k^1 \chi(oooo) - (k^{-1} + k^3 + C''_x k^{-6})\chi(xooo) + k^{-3}\chi(oxoo) + k^6\chi(xoox) = 0 \quad (A10b)$$

$$\dot{\chi}(oxoo) = k^3\chi(xooo) - (k^{-3} + k^4 + C'_x k^7 + C''_x k^{-8}) \cdot \chi(oxoo) + k^{-4}\chi(ooxo) + k^{-7}\chi(xxoo) + k^8\chi(oxox) = 0 \quad (A10c)$$

$$\dot{\chi}(ooxo) = k^4\chi(oxoo) - (k^{-4} + k^5 + C'_x k^9 + C''_x k^{-10}) \cdot \chi(ooxo) + k^{-5}\chi(ooox) + k^{-9}\chi(xoxo) + k^{10}\chi(ooxx) = 0 \quad (A10d)$$

$$\dot{\chi}(ooox) = C''_x k^{-2}\chi(oooo) + k^5\chi(ooxo) - (k^2 + k^{-5} + C'_x k^{11})\chi(ooox) + k^{-11}\chi(xoox) = 0 \quad (A10e)$$

$$\dot{\chi}(xxoo) = C'_x k^7 \chi(oxoo) - (k^{-7} + k^{12} + C''_x k^{-27}) \cdot \chi(xxoo) + k^{-12}\chi(xoxo) + k^{27}\chi(xxox) = 0 \quad (A10f)$$

$$\dot{\chi}(oxxo) = -(k^{-16} + C''_x k^{-19} + C'_x k^{20} + k^{17})\chi(oxxo) + k^{16}\chi(xoxo) + k^{19}\chi(oxxx) + k^{-17}\chi(oxox) + k^{-20}\chi(xxxo) = 0 \quad (A10g)$$

$$\dot{\chi}(ooxx) = C''_x k^{-10}\chi(ooxo) - (k^{10} + k^{-15} + C'_x k^{28}) \cdot \chi(ooxx) + k^{15}\chi(oxox) + k^{-28}\chi(xoxx) = 0 \quad (A10h)$$

$$\dot{\chi}(xoox) = C''_x k^{-6}\chi(xooo) + C'_x k^{11}\chi(ooox) - (k^6 + k^{-11} + k^{-13} + k^{14})\chi(xoox) + k^{13}\chi(xoxo) + k^{-14}\chi(oxox) = 0 \quad (A10i)$$

$$\dot{\chi}(xoxo) = C'_x k^9 \chi(ooxo) + k^{12}\chi(xxoo) + k^{-16}\chi(oxxo) + k^{-13}\chi(xoox) - (k^{-9} + k^{-12} + k^{13} + k^{16} + C''_x k^{-18})\chi(xoxo) + k^{18}\chi(oxxx) = 0 \quad (A10j)$$

Four Site Model
(general)

4 a

Steady State Scheme

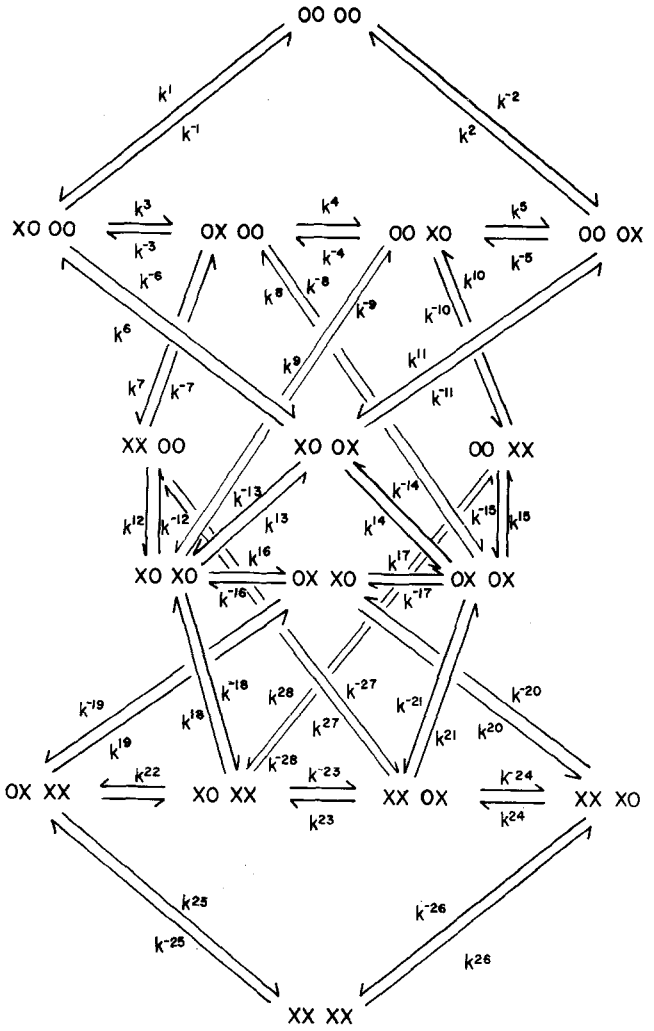

4 b

Energy Profile

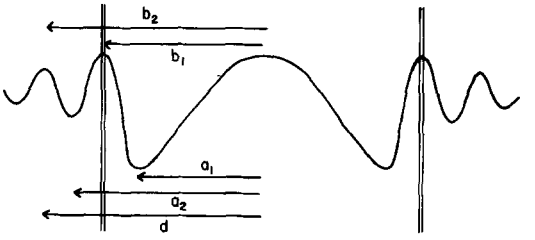

$$\dot{\chi}(o\,x\,o\,x)=C''_x k^{-8}\chi(o\,x\,o\,o)+k^{17}\chi(o\,x\,x\,o)+k^{-15}\chi(o\,o\,o\,x)+k^{14}\chi(x\,o\,o\,x)-(k^{8}+k^{-14}+k^{15}+k^{-17}+C'_x k^{21})\chi(o\,x\,o\,x)+k^{-21}\chi(x\,x\,o\,x)=0 \qquad (A10k)$$

$$\dot{\chi}(x\,x\,x\,o)=C'_x k^{20}\chi(o\,x\,x\,o)-(k^{-20}+k^{24}+C''_x k^{-26})\chi(x\,x\,x\,o)+k^{-24}\chi(x\,x\,o\,x)+k^{26}\chi(x\,x\,x\,x)=0 \qquad (A10l)$$

$$\dot{\chi}(x\,x\,o\,x)=C''_x k^{-27}\chi(x\,x\,o\,o)+C'_x k^{21}\chi(o\,x\,o\,x)+k^{24}\chi(x\,x\,x\,o)-(k^{-21}+k^{-24}+k^{23}+k^{27})\chi(x\,x\,o\,x)+k^{-23}\chi(x\,o\,x\,x)=0 \qquad (A10m)$$

$$\dot{\chi}(x\,o\,x\,x)=C'_x k^{28}\chi(o\,o\,x\,x)+C''_x k^{-18}\chi(x\,o\,x\,o)+k^{23}\chi(x\,x\,o\,x)-(k^{18}+k^{22}+k^{-23}+k^{-28})\chi(x\,o\,x\,x)+k^{-22}\chi(o\,x\,x\,x)=0 \qquad (A10n)$$

$$\dot{\chi}(o\,x\,x\,x)=C''_x k^{-19}\chi(o\,x\,x\,o)+k^{22}\chi(x\,o\,x\,x)-(k^{19}+k^{-22}+C'_x k^{25})\chi(o\,x\,x\,x)+k^{-25}\chi(x\,x\,x\,x)=0 \qquad (A10o)$$

$$\dot{\chi}(x\,x\,x\,x)=C''_x k^{-26}\chi(x\,x\,x\,o)+C'_x k^{25}\chi(o\,x\,x\,x)-(k^{-25}+k^{26})\chi(x\,x\,x\,x)=0. \qquad (A10p)$$

The single-channel current equation at steady state over the major right-hand barrier becomes

$$I_x = ze\{k^5\chi(o\,o\,x\,o) - k^{-5}\chi(o\,o\,o\,x) + k^{17}\chi(o\,x\,x\,o) - k^{-17}\chi(o\,x\,o\,x) + k^{13}\chi(x\,o\,x\,o) - k^{-13}\chi(x\,o\,o\,x) + k^{24}\chi(x\,x\,x\,o) - k^{-24}\chi(x\,x\,o\,x)\}. \quad \text{(A11)}$$

There are a number of physical problems posed by this model. For example, in going from state $o\,x\,o\,x$ to state $o\,o\,x\,x$ there is initially a large distance between the ions and presumably some four or five water molecules interposed and that distance collapses during the single ion translocation. The question is where does the water go if single filing is enforced. They would seem to have to displace the ion in the right-most position. One way out of this problem is to argue that the right-most ion is attached to the outermost carbonyl of the channel and as such (recognizing that the channel is a helix with a 5-Å translation per turn as shown in Fig. 1) the outermost ions need not block the channel and need not, therefore, adhere to single filing.

5. The Four-Site Model with Virtual Weak Sites

The fifth occupancy model treats the situation where a weak site does not occur as a stable occupancy position until the associated tight site is filled. Since the weak site must now be within the major barrier for entry into the channel in order to be stabilized by repulsion from the ion in the associated tight site, the weak sites are considered to be within the channel proper and, of course, no weak site can occur without its paired tight site being filled. Considering as negligible the probability of simultaneous double ion jumps, this gives nine states as shown in Fig. A-5*a* with 26 rate constants and a schematic energy profile of Fig. A-5*b*. The corresponding steady state equations are

$$\dot{\chi}(o\,o\,o\,o) = -(C'_x k^1 + C''_x k^{-2})\chi(o\,o\,o\,o) + k^{-1}\chi(o\,x\,o\,o) + k^2\chi(o\,o\,x\,o) = 0 \quad \text{(A12a)}$$

$$\dot{\chi}(o\,x\,o\,o) = C'_x k^1\chi(o\,o\,o\,o) - (k^{-1} + C'_x k^3 + C''_x k^{-5} + k^{13})\cdot\chi(o\,x\,o\,o) + k^{-13}\chi(o\,o\,x\,o) + k^{-3}\chi(x\,x\,o\,o) + k^5\chi(o\,x\,x\,o) = 0 \quad \text{(A12b)}$$

$$\dot{\chi}(o\,o\,x\,o) = C''_x k^{-2}\chi(o\,o\,o\,o) + k^{13}\chi(o\,x\,o\,o) - (k^2 + k^{-13} + C'_x k^6 + C''_x k^{-4})\chi(o\,o\,x\,o) + k^{-6}\chi(o\,x\,x\,o) + k^4\chi(o\,o\,x\,x) = 0 \quad \text{(A12c)}$$

$$\dot{\chi}(x\,x\,o\,o) = C'_x k^3\chi(o\,x\,o\,o) - (k^{-3} + C''_x k^{-7})\chi(x\,x\,o\,o) + k^7\chi(x\,x\,x\,o) = 0 \quad \text{(A12d)}$$

$$\dot{\chi}(o\,x\,x\,o) = C''_x k^{-5}\chi(o\,x\,o\,o) + C'_x k^6\chi(o\,o\,x\,o) - (k^5 + k^{-6} + C'_x k^9 + C''_x k^{-10})\chi(o\,x\,x\,o) + k^{-9}\chi(x\,x\,x\,o) + k^{10}\chi(o\,x\,x\,x) = 0 \quad \text{(A12e)}$$

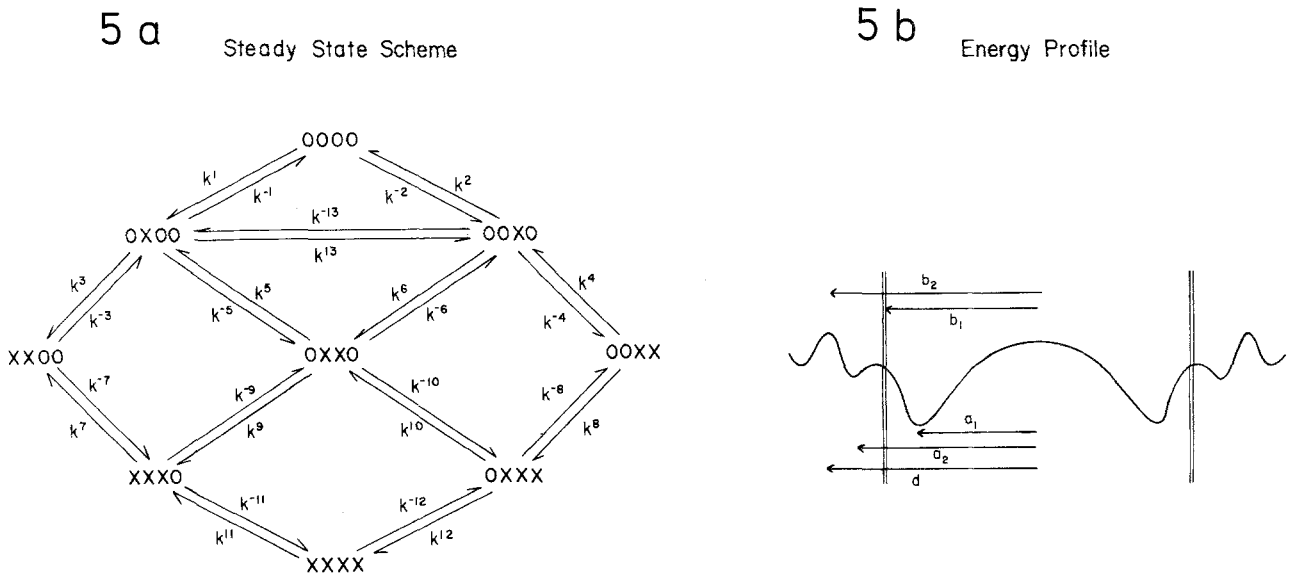

$$\dot{\chi}(o\,o\,x\,x) = C''_x k^{-4}\chi(o\,o\,x\,o) - (k^4 + C'_x k^8)\chi(o\,o\,x\,x) + k^{-8}\chi(o\,x\,x\,x) = 0 \quad \text{(A12}f\text{)}$$

$$\dot{\chi}(x\,x\,x\,o) = C''_x k^{-7}\chi(x\,x\,o\,o) + C'_x k^9 \chi(o\,x\,x\,o) - (k^7 + k^{-9} + C''_x k^{-11})\chi(x\,x\,x\,o) + k^{11}\chi(x\,x\,x\,x) = 0 \quad \text{(A12}g\text{)}$$

$$\dot{\chi}(o\,x\,x\,x) = C''_x k^{-10}\chi(o\,x\,x\,o) + C'_x k^8 \chi(o\,o\,x\,x) - (k^{10} + k^{-8} + C'_x k^{12})\chi(o\,x\,x\,x) + k^{-12}\chi(x\,x\,x\,x) = 0 \quad \text{(A12}h\text{)}$$

$$\dot{\chi}(x\,x\,x\,x) = C''_x k^{-11}\chi(x\,x\,x\,o) + C'_x k^{12}\chi(o\,x\,x\,x) - (k^{11} + k^{-12})\chi(x\,x\,x\,x) = 0. \quad \text{(A12}i\text{)}$$

As before, the expression for the single-channel current is greatly simplified by considering ion movements across a given barrier. Selecting the barrier at the center of the channel for this purpose, the expression for the current becomes

$$I_x = z\,e[k^{13}\chi(o\,x\,o\,o) - k^{-13}\chi(o\,o\,x\,o)] \quad \text{(A13)}$$

while the general expression for the current is

$$\begin{aligned} I_x = \frac{z\,e}{d}\{&[C'_x(d-a_1)k^1 - C''_x(d-a_1)k^{-2}]\chi(o\,o\,o\,o) \\ &+ [C'_x(d-a_2)k^3 - C''_x(d-a_1)k^{-5} \\ &- (d-a_1)k^{-1} + 2a_1 k^{13}]\chi(o\,x\,o\,o) + [(d-a_1)k^2 \\ &- 2a_1 k^{-13} + C'_x(d-a_1)k^6 - C''_x(d-a_2)k^{-4}]\chi(o\,o\,x\,o) \\ &- [C''_x(d-a_1)k^{-7} + (d-a_2)k^{-3}]\chi(x\,x\,o\,o) \\ &+ [(d-a_1)k^5 - (d-a_1)k^{-6} + C'_x(d-a_2)k^9 \\ &- C''_x(d-a_2)k^{-10}]\chi(o\,x\,x\,o) + [(d-a_2)k^4 \\ &+ C'_x(d-a_1)k^8]\chi(o\,o\,x\,x) + [(d-a_1)k^7 \\ &- (d-a_2)k^{-9} - C''_x(d-a_2)k^{-11}]\chi(x\,x\,x\,o) \\ &+ [(d-a_2)k^{10} - (d-a_1)k^{-8} + C'_x(d-a_2)k^{12}] \\ &\cdot\chi(o\,x\,x\,x) + [(d-a_2)k^{11} - (d-a_2)k^{-12}]\chi(x\,x\,x\,x)\}. \end{aligned}$$

Appendix B

Matrix Formulation of the Solution to Steady-State Equations

The steady-state equations of any given multi-site model have the general form

$$\dot{\chi}_i = \sum_{j=o}^{n} q_{ij}\chi_i = 0 \qquad i = 0, 1, 2, n \quad \text{(B1)}$$

where χ_i is the probability of the i^{th} state and q_{ij}'s are the relevant coefficients that will, in general, contain voltage-dependent rate constants and concentration terms. The problem at hand is to compute the numerical values for the probabilities χ_i, given the values of the coefficients, q_{ij}, subject to the conservation condition

$$\sum_{i=o}^{n} \chi_i = 1 \quad \text{(B2)}$$

since the sum of the probabilities of all the states should be unity. This problem is easily solved using simple matrix algebra.

The steady-state equations (B1) consist of $(n+1)$ homogeneous equations in $(n+1)$ unknowns. By ignoring any one of the $(n+1)$ equations, we may derive n *non*-homogeneous equations in n ratios (χ_i/χ_o), $i = 1\,2, \ldots, n$. For instance, ignoring the first equation and taking the χ_o term in each equation to the right-hand side, we have

$$\sum_{j=1}^{n} q_{ij}\chi_j = q_{io}\chi_o \qquad i = 1, 2, \ldots, n \quad \text{(B3)}$$

which may be written in matrix form as

$$\begin{bmatrix} q_{11} & q_{12} \cdots q_{1n} \\ q_{21} & q_{22} \cdots q_{2n} \\ \vdots & \\ q_{n1} & q_{n2} \cdots q_{nn} \end{bmatrix} \begin{bmatrix} \chi_1 \\ \chi_2 \\ \vdots \\ \chi_n \end{bmatrix} = - \begin{bmatrix} q_{10} \\ q_{20} \\ \\ q^{no} \end{bmatrix} \chi_0 . \quad \text{(B4)}$$

This equation is readily solved for the n ratios (χ_i/χ_o), provided the square sub-matrix of order n in (B4) is non-singular:

$$\begin{bmatrix} \chi_1/\chi_o \\ \chi_2/\chi_o \\ \chi_n/\chi_o \end{bmatrix} = - \begin{bmatrix} q_{11} & q_{12} \cdots q_{1n} \\ q_{21} & q_{22} \cdots q_{2n} \\ q_{n1} & q_{n2} \cdots q_{nn} \end{bmatrix}^{-1} \begin{bmatrix} q_{10} \\ q_{20} \\ q_{no} \end{bmatrix}. \quad \text{(B5)}$$

Note that the column vector on the right-hand side of this equation will not be a null vector since it will have at least one nonzero element in it. This is because the coefficients in the $(n+1)$ steady-state equations will appear in pairs so that the χ_o term will appear at least in *two* of the equations. Even if one of them falls out due to one equation being ignored, the other will be present ensuring that the column vector is not a null vector. From Eq. (B5), all the n ratios χ_i/χ_o are obtained. Now, the conservation condition (B2) may be employed in the following form to calculate q_o from the n ratios.

$$1/\chi_o = 1 + \sum_{i=1}^{n} (\chi_i/\chi_o) \quad \text{(B6)}$$

knowing χ_o, all other probabilities χ_i are computed. Thus Eqs. (B5) and (B6) constitute the solution to the problem.

The matrix method was verified by comparison of calculated currents using explicit expressions for the two, and three-site models where the χ_i of Eqs. (A1), (A5), and (A7) were solved for by hand and utilized in an equation of the form (Sandblom et al., 1977)

$$I_x = z\,e\left[\frac{P_1\,C + \ldots + P_n\,C^n}{1 + K_1\,C + \ldots + K_n\,C^n}\right] \qquad \text{(B7)}$$

where n is the maximum occupancy of the channel.

References

Anderson, O.S., Procopio, J. 1980. Ion movement through gramicidin A channels. *Acta Physiol. Scand. (Suppl.) (in press)*

Backer, H.J., Lolkema, J. 1938. Esters of methanetricarboxylic acid. *Rec. Trav. Chim. Pays-Bas* **57**:1234

Bamberg, E., Apell, H.J., Alpes, H. 1977. Structure of the gramicidin A channel: Discrimination between the $\pi_{L,D}$ and the β helix by electrical measurements with lipid bilayer membranes. *Proc. Nat. Acad. Sci. USA* **74**:2402

Bamberg, E., Janko, K. 1977. The action of a carbon-suboxide dimerized gramicidin A on lipid bilayer membranes. *Biochim. Biophys. Acta* **465**:486

Bamberg, E., Kolb, H.-A., Läuger, P. 1976. Ion transport through the gramicidin A channel. *In:* The Structural Basis of Membrane Function. Y. Hatefi and L. Djavadi-Ohaniance, editors. p. 143. Academic Press, New York

Bamberg, E., Läuger, P. 1974. Temperature-dependent properties of gramicidin A channels. *Biochim. Biophys. Acta* **367**:127

Bamberg, E., Läuger, P. 1977. Blocking of the gramicidin channel by divalent cations. *J. Membrane Biol.* **35**:351

Binsch, G. 1968. The study of intramolecular rate processes by dynamic nuclear magnetic resonance. *In:* Topics in Stereochemistry. E.L. Eliel and N.L. Allinger, editors. p. 97. Wiley, New York

Bradley, R.J., Romine, W.O., Long, M.M., Ohnishi, T., Jacobs, M.A., Urry, D.W. 1977. Synthetic peptide K^+ Carrier with Ca^{2+} inhibition. *Arch. Biochem. Biophys.* **178**:468

Bradley, R.J., Urry, D.W., Okamoto, K., Rapaka, R.S. 1978. Channel structures of gramicidin: Characterization of succinyl derivatives. *Science* **200**:435

Bull, T.E. 1972. Nuclear magnetic relaxation of spin-$\frac{3}{2}$ nuclei involved in chemical exchange. *J. Mag. Res.* **8**:344

Bull, T.E., Andrasko, J., Chiancone, E., Forsén, A. 1973. Pulsed nuclear magnetic resonance studies on ^{23}Na, ^{7}Li and ^{35}Cl binding to human oxy- and carbon monooxyhalmoglobin. *J. Mol. Biol.* **73**:251

Chang, D.C., Woessner, D.E. 1978. Spin-echo study of ^{23}Na relaxation in skeletal muscle. Evidence of sodium ion binding inside a biological cell. *J. Mag. Res.* **30**:185

Chock, P.B., Eggers, F., Eigen, M., Winkler, R. 1977. Biophys. Chem. **6**:239

Cornélis, A., Laszlo, P. 1979. Sodium binding sites of gramicidin A: Sodium-23 nuclear magnetic resonance study. *Biochemistry* **10**:2004

Delville, A., Detellier, C., Laszlo, P. 1979. Determination of the correlation time for a slowly reorienting spin $-\frac{3}{2}$ nucleus: Binding of Na^+ with the 5'-GMP supramolecular assembly. *J. Mag. Res.* **34**:301

Eisenman, G., Sandblom, J., Neher, E. 1977. Ionic selectivity, saturation, binding and block in the gramicidin A channel: A preliminary report. *In:* Metal-Ligand Interactions in Organic Chemistry and Biochemistry. B. Pullman and N. Goldblum, editors. Part 2, p. 1. D. Reidel, Dordrecht-Holland

Eisenman, G., Sandblom, J., Neher, E. 1978. Interactions in cation permeation through the gramicidin channel Cs, Rb, K, Na, Li, Tl, H and effects of anion binding. *Biophys. J.* **22**:307

Eyring, H., Urry D.W. 1963. The theory of absolute reaction rates in solution. *Ber. Bunsenges. Phys. Chem.* **67**:731

Eyring, H., Urry, D.W. 1965. Thermodynamics and chemical kinetics. *In:* Theoretical and Mathematical Biology. H.J. Morowitz and T.H. Waterman, editors. p. 57. Blaisdell, New York

Feeney, J., Batchelor, J.G., Albrand, J.P., Roberts, G.C.K. 1979. The effects of intermediate exchange processes on the estimation of equilibrium constants by NMR. *J. Magn. Reson.* **33**:519

Hägglund, J., Enos, B., Eisenman, G. 1979. Multi-site, multi-barrier, multi-occupancy models for the electrical behavior of single filing channels like those of gramicidin. *Brain Res. Bull.* **4**:154

Hladky, S.B., Urban, B.W., Haydon, D.A. 1979. Ion movements in pores formed by gramicidin A. *In:* Membrane Transport Processes. C.F. Stevens and R.W. Tsien, editors. Vol. 3, p. 89. Raven Press, New York

Hubbard, P.S. 1970. Nonexponential nuclear magnetic relaxation by quadrupole interactions. *J. Chem. Phys.* **53**:985

Ishii, S., Witkop, B. 1964. Gramicidin A. II. Preparation and properties of "Seco-Gramicidin A". *J. Am. Chem. Soc.* **86**:1848

James, T.L., Nogle, J.H. 1969. ^{23}Na nuclear magnetic resonance relaxation studies of sodium interaction with soluble RNA. *Proc. Nat. Acad. Sci. USA* **62**:644

Johnson, F.H., Eyring, H., Polissar, M.I. 1954. Potential barriers in diffusion. *In:* The Kinetic Basis of Molecular Biology. Chapter 14. John Wiley & Sons, New York

Koeppe, R.E., II, Berg, J.M., Hodgson, K.O., Stryer, L. 1979. Gramicidin A crystals contain two cation binding sites per channel. *Nature (London)* **279**:723

Kolb, H.-A., Läuger, P., Bamberg, E. 1975. Correlation analysis of electrical noise in lipid bilayer membranes: Kinetics of gramicidin A channels. *J. Membrane Biol.* **20**:133

McBride, D., Szabo, G. 1978. Influence of double-layer and dipolar surface potentials on ionic conductance of gramicidin channels. *Biophys. J.* **21**:A25

Mueller, P., Rudin, D.O. 1967. Development of K^+-Na^+ discrimination in experimental biomolecular lipid membranes by macrocyclic antibiotics. *Biochem. Biophys. Res. Commun.* **26**:398

Neher, E. 1975. Ionic specificity of the gramicidin channel and the thallous ion. *Biochim. Biophys. Acta* **401**:540

Norne, J.E., Gustabsson, H., Forsen, S., Chiancone, E., Kuiper, H.A., Antonini, E. 1979. Sodium and calcium binding to panulirus interruptus hemocyanin as studied by ^{23}Na nuclear magnetic resonance. *Eur. J. Biochem.* **98**:591

Parihar, D.P., Sharma, S.P., Verma, K.K. 1967. Studies of some active methylene compounds by thin-layer chromatography. *Chromatog.* **27**:276

Parlin, B., Eyring, H. 1954. Membrane permeability and electrical potential. *In:* Ion Transport Across Membranes. H.T. Clarke, editor, p. 103. Academic Press, New York

Pople, J.A., Schneider, W.G., Bernstein, H.J. 1959. High resolution nuclear magnetic resonance. *In:* High-Resolution Nuclear Magnetic Resonance, p. 218. McGraw-Hill, New York

Sandblom, J., Eisenman, G., Neher, E. 1977. Ion selectivity, saturation and block in gramicidin A channels: I. Theory for the electrical properties of ion selective channels having two pairs of binding sites and multiple conductance states. *J. Membrane Biol.* **31**:383

Sarges, R., Witkop, B. 1964. Gramicidin A. IV. Primary sequence of valine and isoleucine gramicidin A. *J. Am. Chem. Soc.* **86**:1862

Urban, B.W., Hladky, S.B., Haydon, D.A. 1978. The kinetics of ion movements in the gramicidin channel. *Fed. Proc.* **37**:2628

Urry, D.W. 1971. The gramicidin A transmembrane channel: A proposed $\pi_{(L,D)}$ helix. *Proc. Nat. Acad. Sci. USA* **68**:672

Urry, D.W. 1973. Polypeptide conformation and biological function β-helices ($\pi_{L,D}$-helices) as permselective transmembrane channels. *In:* Conformation of Biological Molecules and Polymers – The Jerusalem Symposia on Quantum Chemistry and Biochemistry. V, p. 723. Israel Academy of Sciences, Jerusalem

Urry, D.W. 1978. Basic aspects of calcium chemistry and membrane interaction: On the messenger role of calcium *Ann. N.Y. Acad. Sci.* **307**:3

Urry, D.W., Goodall, M.C., Glickson, J.D., Mayers, D.F. 1971. The gramicidin A transmembrane channel: Characteristics of head to head dimerized $\pi_{(L,D)}$ helices. *Proc. Nat. Acad. Sci. USA* **68**:1907

Urry, D.W., Long, M.M., Jacobs, M., Harris, R.D. 1975. Conformation and molecular mechanisms of carriers and channels. *Ann. NY Acad. Sci.* **264**:203

Urry, D.W., Spisni, A., Khaled, M.A. 1979*a*. Characterization of micellar-packaged gramicidin A channels. *Biochem. Biophys. Res. Commun.* **88(3)**:940

Urry, D.W., Spisni, A., Khaled, M.A., Long, M.M., Masotti, L. 1979*b*. Transmembrane channels and their characterization in phospholipid structures. *Int. J. Quantum Chem.:* Quantum Biology Symp. N. **6**:289

Urry, D.W., Venkatachalam, C.M., Spisni, A., Läuger, P., Khaled, M.A. 1980. Rate theory calculation of gramicidin single channel currents using NMR-derived rate constants. *Proc. Nat. Acad. Sci. USA* **77**:2028

Weinstein, S., Wallace, B., Blout, E.R., Morrow, J.S., Veatch, W. 1979. Conformation of gramicidin A channel in phospholipid vesicles: A ^{13}C and ^{19}F nuclear magnetic resonance study. *Proc. Nat. Acad. Sci. USA* **76**:4230

Zwolinski, B.I., Eyring, H., Reese, C.E. 1949. Diffusion and membrane permeability. *J. Phys. Chem.* **53**:1426

Received 10 January 1980